

國立交通大學

材料科學與工程學系 奈米科技碩士班

碩士論文

玫瑰之吻：受生物啟發具有超疏水和高水滴吸附力之表面並

應用於未來之無殘留轉印技術

**Kiss from a Rose: Bioinspired Superhydrophobic and High-Water
Adhesive Surface for Future Nonresidual Imprint Technique**

研究生：林易成 Yi-Cheng Lin

指導教授：柯富祥 教授 Prof. Fu-Hsiang Ko

中華民國九十九年八月

玫瑰之吻：受生物啟發具有超疏水和高水滴吸附力之表面並
應用於未來之無殘留轉印技術

**Kiss from a Rose: Bioinspired Superhydrophobic and High-Water
Adhesive Surface for Future Nonresidual Imprint Technique**

研究生：林易成

Student : Yi-Cheng Lin

指導教授：柯富祥 教授

Advisor : Prof. Fu-Hsiang Ko

國立交通大學

材料科學與工程學系奈米科技碩士班



碩 士 論 文

A Thesis

Submitted to Institute of Nanotechnology
Department of Materials Science and Engineering

College of Engineering

National Chiao Tung University

in partial Fulfillment of the Requirements

for the Degree of

Master

in

Nanotechnology

August 2010

Hsinchu, Taiwan, Republic of China

中華民國九十九年八月

Acknowledgment

感謝柯富祥教授在學生的碩士生涯期間給予最充份的指導，並提供豐富的實驗環境與資源，讓我們能無後顧之憂地全心專注於實驗上，此外於學術外與生活上的關心，亦培養我們健全的人格，使我們不至於在實驗之中迷失了自我，在專業領域及待人處事上都有均衡的發展。

時間過得很快，一轉眼間兩年的光陰就過了，回首過往的日子，有快樂、有難過，但總有大家一路相扶持。很感謝又帥又迷人的佳典學長、中書學長和捷學長在每星期都能撥冗聽聽我們的報告，並適時的給予我許多指教，有時候實驗方向迷失了，好在有你們在實驗的路上給予寶貴的建議。實驗室也就像是一個大家庭，他就像是我在新竹的家，每每有事情總有許多實驗室的朋友會伸出援手。於此我要特別謝謝大家，如果沒有大家的幫忙，在實驗的路上將會是徬徨而孤單。

感謝崇志、懷箴、品樺、丁香，有你們的實驗室總是讓人備感溫暖，熱心助人的品樺、丁香，以及逗趣風雅的崇志和頭頭是道的懷箴。另外也要感謝其昌學長、俊淇學長、銘清學長、京璋學長、嘉琦學姐、玫菲學姐、伯軒學長實驗室也因為你們而更有秩序，從你們的身上看到了許多的優點值得我去學習。當然實驗室的新學弟妹，也因為你們的熱情，讓我們實驗室多了好多的歡笑；于菱、大軒、琬婷、怡君、韋伶在未來實驗室的氛圍要由你們來營造，相信你們可以做得很好。

除了感謝實驗室的人，我也要謝謝和我一起來新竹念書的大學朋友們，謝謝冠倫和毓倫，在經歷了許多我人生很重要的轉捩點有你們一路相陪伴。也要特別感謝家人的支持與鼓勵，媽媽、妹妹、祖母以及在天國的爸爸，有長輩們的諄諄教誨才会有現在的我，每當累到想放棄，每當心情不好時，你們總是敞開著雙手在家歡迎我，家是一個我最重要的避風港，有了安全舒適的居所，我才能夠勇往直前。最後我也要感謝以前教導過我的老師們，哪怕是任何一句受用的話，都再再影響我深遠。

玫瑰之吻：受生物啟發具有超疏水和高水滴吸 附力之表面並應用於未來之無殘留轉印技術

研究生：林易成

指導教授：柯富祥 教授

國立交通大學材料科學與工程學系奈米科技碩士班

摘要

自從蓮葉效應被發現後，許多受生物啟發的超疏水表面其具備自潔淨特性者已經被大量製造。然而，最近幾年科學家被玫瑰花表面所深深吸引，其表面具有超疏水的特性和高水滴吸附力。此種現象是由花瓣上面微米尺度的凸起和奈米結構所產生。直至今日，許多研究者仍不知如何去製造出此等複雜的結構並使其真正拿來應用。為了去仿製花瓣的表面，我們發展出一種由下而上的方法：藉由簡單的酸雕刻技術來製作具有高水滴吸附力和自潔淨特性的超疏水聚二甲基矽氧烷(PDMS)。此類花瓣的聚二甲基矽氧烷具有35微米的寬度、奈米皺褶約在500奈米和小於100奈米的奈米結構。在長時間的檢測下，其也能展現大於150度的水滴接觸角。這些結論僅來自於其表面形貌的改變而與化學修飾並不相關。其展現的超疏水特性至少能維持一個月。此外，pH值從1到14、具有腐蝕性的水溶液在聚二甲基矽氧烷表面上也可以展現出高的水滴接觸角。更甚者，此類花瓣展現了高水滴吸附力達到 35.81 N/m^2 。我們使用此類花瓣聚二甲基矽氧烷當作一個具黏性的手掌來搬運一5 mg的水滴，從一起疏水和自潔淨的聚二甲基矽氧烷表面搬運至親水的矽晶圓表面上。除此之外，從酸雕刻技術得來的兩種超疏水表面讓我們得以用來製造一個新型無殘留的印章。其超疏水且對水滴具吸附力的區域可用於將染料從印章轉移至紙上。而超疏水具備自潔淨的區域可以避免染料沾附上去。

以此方式，這種新世代的超疏水表面能夠廣泛的使用在生物科技、微流體系統和工業領域。



Kiss from a Rose: Bioinspired Superhydrophobic and High-Water Adhesive Surface for Future Nonresidual Imprint Technique

Student: Yi-Cheng Lin

Advisor: Prof. Fu-Hsiang Ko

Department of Materials Science and Engineering
Institute of Nanotechnology
National Chiao Tung University

Abstract

Many bio-inspired superhydrophobic surfaces with self-cleaning property have been fabricated since “Lotus effect” was discovered. However, scientists were fascinated by the petal’s surface which has superhydrophobicity and high water adhesion in recent years. The phenomenon is induced by the microscale convex and nanostructures upon the petal. So far, researchers have perplexed how to manufacture the complicated topography and applied it to reality. To mimic the petal’s surface, we developed a bottom-up method by the simple acid texture technique to fabricate the superhydrophobic PDMS surface with high water adhesion and self-cleaning ability. The resulting petal-like PDMS had convexes about 35 μm in diameter, nanowrinkles around 500 nm in width and nanostructures less than 100 nm. A high water contact angle larger than 150° was displayed, even after a long-time duration test. These results caused only by morphology changing instead of chemical modification. The superhydrophobicity could maintain at least a month. Besides, the corrosive solutions range from pH value 1 to 14 also displayed high contact angles on the PDMS surface.

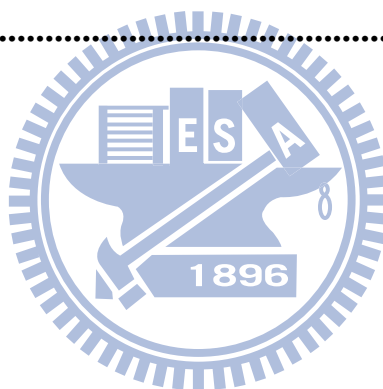
Moreover, the petal-like PDMS exhibited the high water adhesion up to 35.81 N/m^2 . We used the petal-like PDMS surface as a sticky palm to transport a 5 mg water droplet from the superhydrophobic and self-cleaning PDMS to the hydrophilic silicon wafer. In addition, the two superhydrophobic surfaces from the acid texture technique allowed us to fabricate a modern nonresidual stamp. The superhydrophobic and water adhesive area is applicable to transport the dye from the stamp to a paper. The superhydrophobic and self-cleaning region avoids the adhesion of dye. Thus, the new-generation superhydrophobic surface can be widely applied to biotechnology, MEMS and industry.



Contents

Acknowledgment.....	i
Abstract in Chinese.....	ii
Abstract in English	iv
Contents	vi
List of Tables	viii
List of Figures	ix
Chapter 1: Introduction	1
1.1 Learn a lesson from nature	1
1.2 What do we need for a superhydrophobic surface?	6
1.2.1 General wetting states introduction	6
1.2.1.1 Wenzel model of wetting of rough surfaces	6
1.2.1.2 Cassie-Baxter model of wetting of rough surfaces.....	7
1.2.2 Lotus effect-a superhydrophobic and self-cleaning surface.....	9
1.2.3 Petal effect-a superhydrophobic and high adhesive surface.....	11
Chapter 2: Literatures Review	13
2.1 Superhydrophobic surfaces with high adhesive force for water	13
2.1.1 Hairy-type structure	13
2.1.2 Tube-type structure	16
2.1.3 Convex-type structure	18
2.1.4 Other type structure	22
2.2 Motivation.....	23
Chapter 3: Experimental Section	25
3.1 General Introduction	25
3.2 Flat PDMS with periodic wrinkles	27
3.3 Petal-like PDMS surface manufacture.....	27
3.4 Fresh rose petal and chrysanthemum petal dehydration.....	28
3.5 Specimen characterization	30
Chapter 4: Results and Discussion	32
4.1 The results of periodic wrinkles on plane PDMS.....	32
4.1.1 Surface topography.....	32

4.1.2 Mechanism of resulting periodic wrinkles.....	37
4.1.3 Chemical functional group analysis	39
4.1.4 Wetting phenomenon of the surface.....	42
4.2 Petal-like surface characterization.....	46
4.2.1 Three level structures analysis.....	47
4.2.2 Cassie impregnating wetting state	50
4.2.3 High adhesive forces for water	51
4.3 Innovative application of petal-like surface	55
4.3.1 A sticky palm for water transportation	55
4.3.2 A nonresidual stamp for imprint technique	56
 Chapter 5: Conclusion.....	 58
 Reference.....	 59



List of Tables

Table 4.133

The reaction conditions were listed above, in which, S/N presented the volume ratio of sulfuric acid over nitric acid, #1~#8 represented serious samples' numbers, first column indicated the reaction time, all the samples reaction at 55°C; after acid corrosion, samples was cooled by cold water for 30 seconds at 2°C~3°C.

Table 4.241

Expected absorption band in FT-IR spectra of PDMS and common functional groups.

Table 4.354

The wetting properties of different structure levels.



List of Figures

Figure 1.12

Multi-scale structures in biology. Four types of interesting biological properties can be found in nature: (a) Self-cleaning properties: lotus leaf, duck feather, and mosquito eye (from left to right). (b) Mechanical properties: gecko feet, octopus suckers, and water strider. (c) Color through structure: peacock feather, butterfly wings, and beetle shells. (d) Optical properties: cicada wings, moth compound eyes, and sponge spurs. In each case the first row shows a photograph of the biological feature, while the second and third rows show scanning electron microscopy (SEM) images of corresponding micro- and nanometer-scale structures.

Figure 1.23

The water-capturing surface of the fused overwings (elytra) of the desert beetle *Stenocara* sp. (a) Adult female, dorsal view; peaks and troughs are evident on the surface of the elytra. (b) A 'bump' on the elytra, stained with Red O for 15 min and then with 60% isopropanol for 10 min, a procedure that tests for waxes. Depressed areas of the otherwise black elytra are stained positively (waxy, coloured), whereas the peaks of the bumps remain unstained (wax-free; black). (c) Scanning electron micrograph of the textured surface of the depressed areas. Scale bars: a, 10 mm; b, 0.2 mm; c, 10 μ m.

Figure 1.34

Structure of wet-rebuilt spider silk. (a) Environmental SEM image of periodic spindle-knots linking with slender joints. The apex angle of spindle-knots (2β) is about 19° . Low-magnification (b) and zoomed (c) images show that the spindle-knot is randomly interweaved by nanofibrils. Low-magnification (d) and high-magnification (e) images of the joint, which is composed of nanofibrils aligned relatively parallel to the silk axis.

Figure 1.45

Gecko setae and apparatus for force measurement. (a) Tokay gecko (*Gekko gecko*) with toe outlined. SEM images of rows of setae from a toe (b), a single seta (c) and, the finest terminal branches of a seta, called spatulae (d). (e) Single seta attached to a micro-electromechanical system (MEMS) cantilever capable of measuring force production during attachment parallel and perpendicular to the surface. (f) Single seta attached to an aluminum bonding wire capable of measuring force production during detachment perpendicular to the surface. The angle between setae stalk and the wire is

represented in α .

Figure 1.5 9

A liquid droplet in contact with (a) a smooth solid surface (b), (c) a rough solid surface. (b) Illustrate Wenzel's wetting state. (c) Illustrate Cassie's wetting state.

Figure 1.6 11

Superhydrophobic and self-cleaning surfaces. A flowering plant of Lotus (*Nelumbo nucifera*) is shown in (a). A Lotus leaf contaminated with clay (b) and removal of the adhering particles by water (c). (d) A spherical water droplet on a superhydrophobic leaf is shown. (e) SEM micrograph of a droplet illustrates the low wettability of superhydrophobic microstructured surfaces. The SEM micrographs show the Lotus leaf surface in different magnifications: (f) randomly distributed cell papilla, (g) a detail of the cell papilla and (h) the epicuticular wax tubules on the cells are shown.

Figure 1.7. 12

(a), (b) SEM images of the surface of a red rose petal, showing a periodic array of micropapillae and nanofolds on each papillae top.

Figure 2.1 15

FE-SEM images of AAO templates anodized at the second anodization for (a) 10 min and (b) 20 min, and their h-PDMS replicas. The bottom shows a static water contact angle on the each replica surface. The scale bar is 500 nm.

Figure 2.2 15

Shapes of a water droplet on the fabricated, hairy h-PDMS nanopillar surface with different tilt angles: (a) 90° and (b) 180°.

Figure 2.3 16

(a) Cross-sectional SEM image of the structured PPX-COCF₃ film. Shapes of water droplets on the structured PPX-COCF₃ film with different tilt angles: (b) 0°, (c) 90°, and (d) 180°.

Figure 2.4 17

SEM images of PS nanotubes of (a) top view, (b) magnified image of (a), (c) side view and (d) the contact angle behavior.

Figure 2.5 18

(a), (b) Top-view and side-view SEM images of superhydrophobic TiO₂ NTA nanostructures. The inset is a photo of a water droplet on the superhydrophobic NTA surface with diameters of 78 ± 14 nm. (c), (d) The curves of water contact angles and adhesive force on the superhydrophobic NTA nanostructures with respect to the diameter and length of nanotubes.

Figure 2.619

(a), (b) The microlens-arrayed surface morphology was apparent at high magnification.

Figure 2.719

The adhesive force of a microlens array. (a), (b) Behavior of a water droplet on a 10×6 microlens-arrayed surface with tilt angles of 90° and 180° , respectively. (c) The work of adhesion (open symbol) and contact angle (solid symbol) as a function of the drop volume on the PDMS with flat surface (square), 10×2 array (circle), and 10×6 array (triangle). The work of adhesion was obtained directly from the contact-angle measurements. The insets show a cross-sectional view of the SEM images of the microlens array with different heights.

Figure 2.820

(a), (b) SEM images of the duplicated PVA film with inverse petal structures. (c), (d) SEM images of the duplicated PS film with the similar petal's surface structures. (Inset in panel d is the shape of a water drop on the PS film when it is turned upside down, indicating its superhydrophobic adhesive property.)

Figure 2.920

The water could permeate into the grooves of the surface. A droplet of water could pin on the replicated surface because of strong capillary forces.

Figure 2.1021

SEM image of the lycopodium-based substrate. The lycopodium particles were spread uniformly, the particles' sizes were quite similar about $30 \mu\text{m}$ in diameter, and the minimal pore size was $5 \mu\text{m}$.

Figure 2.1122

Water droplets ($10 \mu\text{L}$) attached to vertical (a) and horizontal (c) lycopodium-based surfaces. (b) Water droplet ($40 \mu\text{L}$) deposited on the lycopodium-based surface.

Figure 2.1223

Directional adhesion on superhydrophobic butterfly wings and SEM images of the wings: (a) an iridescent blue butterfly (*Morpho aega*); the black arrows denote the RO direction away from the body's center axis; (b) the droplet easily rolls along the RO direction when the wing is tilted toward downward by 9°; (c) the droplet pinned on the wing that is tilted upward; (d) (e) SEM images of the wings (scale bars = (d) 100 μm and (e) 100 nm). (f) (g) two models proposed for the potential mechanism of distinct adhesions (f) rolling state and (g) pinning state.

Figure 3.129

The flow chart of preparing the superhydrophobic PDMS surface.

Figure 3.229

The scheme showed the protocol of manufacturing a petal-like PDMS.

Figure 4.134

Optical microscopy images of the PDMS going through acid, mixture of sulfuric acid and nitric acid under the 1/1 volume ratio, corrosion with different treatment times of (a) 5 s, (b) 15 s, (c) 30 s, and (d) 60 s.

Figure 4.235

Optical microscopy images of the PDMS going through acid, mixture of sulfuric acid and nitric acid under the 2/1 volume ratio, corrosion with different treatment times of (a) 5 s, (b) 15 s, (c) 30 s, and (d) 60 s.

Figure 4.336

Scheme showed the periodic wrinkles resulted from the increasing immersion time at different acid composition of sulfuric acid/nitric acid = 1/1 and 2/1 in volume ratio.

Figure 4.436

The scheme indicated that width of the periodic wrinkles at the same corrosion time was proportional to the reaction temperature. The acid was composited of sulfuric acid and nitric acid in a volume ratio of 1/1.

Figure 4.537

The PDMS treated with acid producing a superhydrophobic and non-sticky

surface. (a) Optical microscope image of periodic wrinkles PDMS caused by acid corrosion. (b), (c) SEM images showing two scales, micro- and nano-, structures. (d) A 5 mg water droplet located on the superhydrophobic and non-sticky PDMS surface, showing a contact angle of 151.5°.

Figure 4.639

The formation mechanism of periodic wrinkles under a flat PDMS. A flat PDMS was fixed onto a clean wafer then undergone an acid corrosion. Outer layer of PDMS was reacted by acid which caused a different thermal expansion coefficient between inner layer (bulk PDMS) and outer layer (Reaction region). During cooling process, it formed periodic wrinkles.

Figure 4.742

An scheme indicated the FT-IR spectra of PDMS surface (a) comparison (b), (c) and (d); (b) no treatment and (c) treated by pure sulfuric acid (d) treated by mixture acid, sulfuric acid/nitric acid = 1/1 in volume ratio.

Figure 4.844

(a)-(n) Images showed the contact angle changed from different condition solution, pH values changed from 1-14. The superhydrophobic property of the treated PDMS surface maintained as similar as the pure water. A high contact angle around 150° was revealed during the wide range of pH values.

Figure 4.945

Images showed the wetting phenomena of different pH values of solutions.

Figure 4.1045

Graph showing the relationship between time and contact angle on the treated PDMS.

Figure 4.1147

The SEM images of dehydrated (a), (b) a rose-petal and (c), (d) a chrysanthemum-petal, the surface showed the large-scaled convex and the nano-fold. The convex structure is about 20~30 μm in width and the nano-fold is less than 1 μm μm.

Figure 4.1248

Scheme showed the formation of PS spheres assembled on a silicon wafer caused

by the water flow.

Figure 4.1349

(a) The SEM image show the close-packed convex. (b), (c) Showing SEM images for the manufactured surface with the topography which was similar to the rose-petal. (d) SEM image indicated the nanostructure of the surface.

Figure 4.1449

Scheme showed the three level structures on PDMS.

Figure 4.1551

A 5 mg water droplet pinned on (a) a flat PDMS surface, (b) a PDMS with micro-scaled convex, and (c), (d) a PDMS surface with petal-like morphology when turning the surface vertically (90°) and upside (180°) respectively.

Figure 4.1651

Water penetrating the microscale convex and partial wetting the upper part of nanoscale wrinkles.

Figure 4.1753

The graph of water contact angles and adhesive force between different morphology, flat, micro-scaled convex and petal-like topography.

Figure 4.1854

The histogram of water contact angles and adhesive forces on the petal-like surface changed with decanting times. Blue rectangles indicated that adhesive force increased from 28.89 N/m^2 to 35.81 N/m^2 . Orange rectangles showed the contact angle changed from 137.93° to 150.01° .

Figure 4.1955

A 5 mg water droplet transported from a hydrophobic and non-sticky surface to a hydrophilic surface by the petal-like surface PDMS.

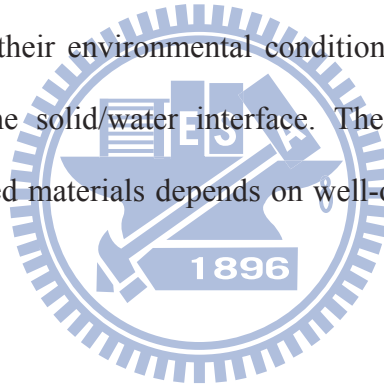
Figure 4.2057

(a) Scheme indicated the two different superhydrophobic surfaces on the PDMS. (b) Several hundreds of patterns on the paper by using the fabricated PDMS stamp. (c) The image showed the PDMS stamp remained cleaning after using many times.

Chapter 1: Introduction

1.1 Learn a lesson from nature

Learning from Nature means taking ideas from Nature and developing novel functional materials. These bioinspired, smart materials are attracting more and more interest because of their unique properties, which have paved the way to many real-world applications, e.g., biomimetic fins [1], actively moving polymers [2], neural memory devices [3], smart micro-/nano-containers for drug delivery [4], various biosensors [5, 6], dual/multi-responsive materials [7, 8]. Also, many of these smart materials have surfaces that dynamically alter their physicochemical properties in response to changes in their environmental conditions and a triggered control of interfacial properties at the solid/water interface. The creation of such complex functionalities in bioinspired materials depends on well-ordered multiscale structures showed in Figure 1.1 [9].



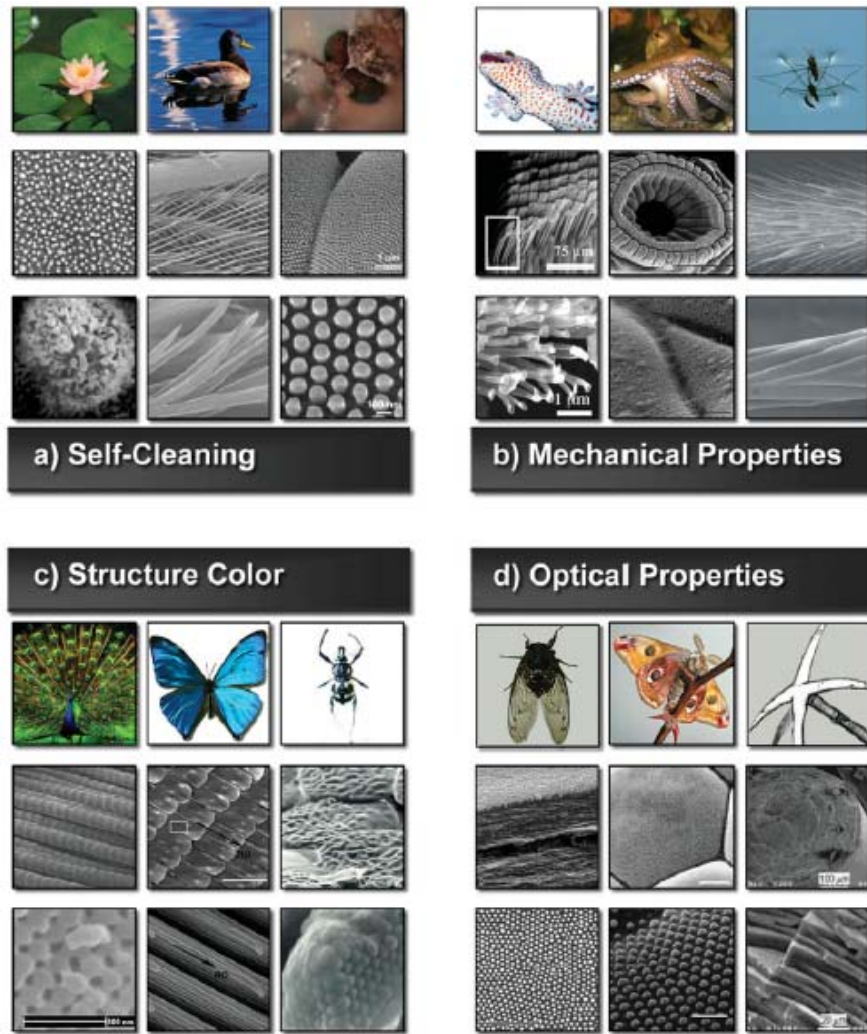


Figure 1.1 Multi-scale structures in biology. Four types of interesting biological properties can be found in nature: (a) Self-cleaning properties: lotus leaf, duck feather, and mosquito eye (from left to right) (b) Mechanical properties: gecko feet, octopus suckers, and water strider (c) Color through structure: peacock feather, butterfly wings, and beetle shells and (d) Optical properties: cicada wings, moth compound eyes, and sponge spur. In each case the first row shows a photograph of the biological feature, while the second and third row show scanning electron microscopy (SEM) images of corresponding micro- and nanometer-scale structures.

Many biological surfaces in both the plant and animal kingdom possess unusual structural features at the micro- and nano-scale that control their interaction with

water and hence wettability [10-14]. An intriguing example is provided by desert beetles (Figure 1.2 [15]), which use micrometre-sized patterns of hydrophobic and hydrophilic regions on their backs to capture water from humid air [15].

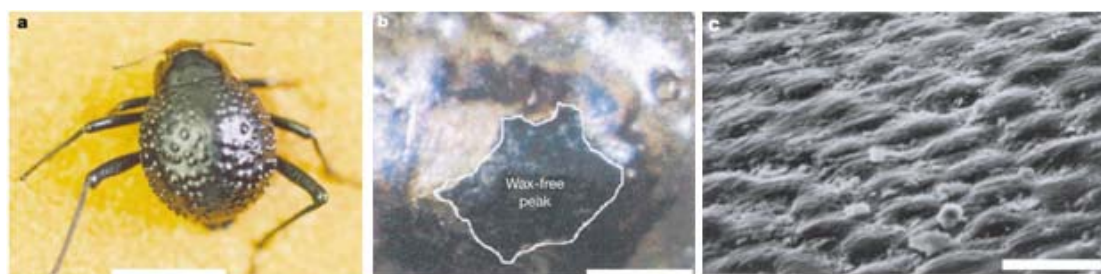


Figure 1.2 The water-capturing surface of the fused overwings (elytra) of the desert beetle *Stenocara* sp. (a) Adult female, dorsal view; peaks and troughs are evident on the surface of the elytra. (b) A ‘bump’ on the elytra, stained with Red O for 15 min and then with 60% isopropanol for 10 min, a procedure that tests for waxes. Depressed areas of the otherwise black elytra are stained positively (waxy, coloured), whereas the peaks of the bumps remain unstained (wax-free; black). (c) Scanning electron micrograph of the textured surface of the depressed areas. Scale bars: (a) 10 mm; (b) 0.2 mm; (c) 10 mm.

Spider silk’s structure (Figure 1.3 [16]) has been studied extensively for its incredible strength and flexibility. Anyone who has seen a spider web after the early morning dew will have noticed water droplets strung along its fine threads. Recently Jiang, a chemist, found that it could have implications for the design of materials for water collection and the efficiency of chemical reactions [16].

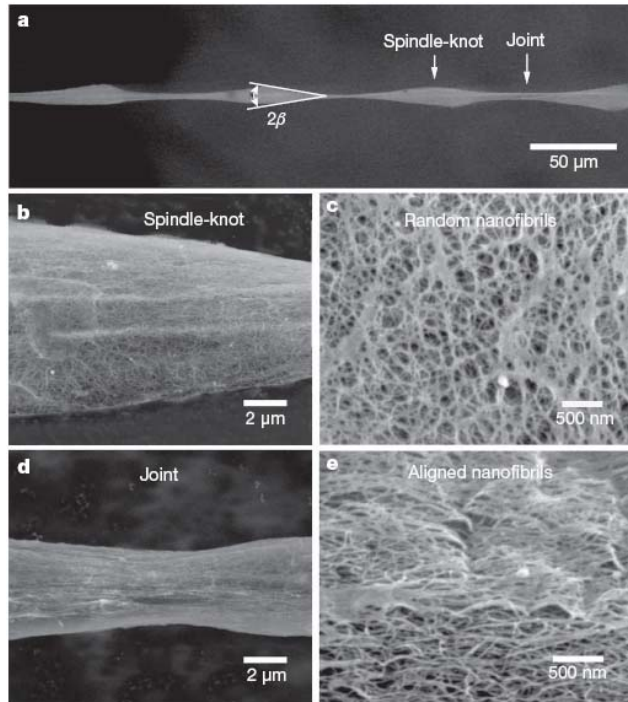


Figure 1.3 Structure of wet-rebuilt spider silk. (a) Environmental SEM image of periodic spindle-knots linking with slender joints. The apex angle of spindle-knots (2β) is about 19° . Low-magnification (b) and zoomed (c) images show that the spindle-knot is randomly interweaved by nanofibrils. Low-magnification (d) and high-magnification (e) images of the joint, which is composed of nanofibrils aligned relatively parallel to the silk axis.

The unusual ability of gecko lizards to climb on any vertical surface and hang from a ceiling with one toe has inspired scientific interest for decades. Only in the past few years a progress has been made in understanding the mechanism that allows the gecko to defy gravity in climbing vertical surfaces. Recent studies revealed the remarkable gecko foot with countless specialized keratinous aligned microscopic elastic hairs (3 to 130 μm in length), called setae (Figure 1.4 [17]), splitting into even smaller spatula (0.2 to 0.5 μm in diameter) at the end. The adhesive force is caused by these spatulae that come in close contact with the surface to induce strong van der Waals (vdW) forces ($\sim 10 \text{ N cm}^{-2}$) to hold gecko lizards onto a vertical wall [17, 18].

By using carbon nanotube arrays that are dominated by a straight body segment but with curly entangled top, Qu, et al. have created gecko-foot-mimetic dry adhesives that show macroscopic adhesive forces of $\sim 100 \text{ N/cm}^2$, almost 10 times that of a gecko foot, and a much stronger shear adhesion force than the normal adhesion force [19].

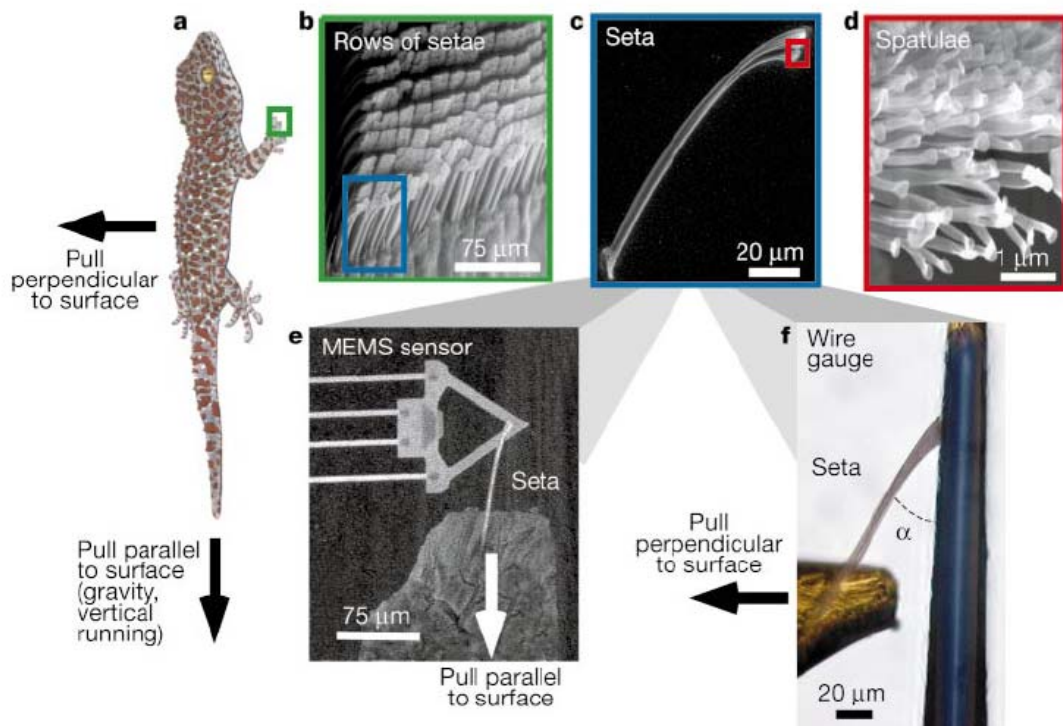


Figure 1.4 Gecko setae and apparatus for force measurement. (a) Tokay gecko (*Gekko gekko*) with toe outlined. SEM images of rows of setae from a toe (b), a single seta (c) and, the finest terminal branches of a seta, called spatulae (d). (e) Single seta attached to a micro-electromechanical system (MEMS) cantilever capable of measuring force production during attachment parallel and perpendicular to the surface. (f) Single seta attached to an aluminum bonding wire capable of measuring force production during detachment perpendicular to the surface. The angle between setae stalk and the wire is represented in α .

Approximately 460 million years ago, the first plants moved from their aqueous environment to the drier atmosphere on land, and they needed a protective outer coverage. The development of the cuticle as hydrophobic outer coverage was one of the key innovations that enabled plants to leave their primarily aquatic habitat and to overcome the physical and physiological problems connected to an ambient environment, such as desiccation. Some naturally occurring plant leaves such as those of the lotus have well-demonstrated superhydrophobic surfaces such that water drops can easily roll off and carry away dust particles and debris, a mechanism often referred to as self-cleaning [20-22]. The self-cleaning of lotus leaves in particular is a popular topic of study because of the observed wetting properties of the material surfaces [23-25].

1.2 What do we need for a superhydrophobic surface?

Superhydrophobic surfaces have drawn a lot of interest both in academia and in industry. These surfaces are of special interest, because properties such as anti-sticking, anti-contamination [26], and self-cleaning [27, 28] are expected.

1.2.1 General wetting states introduction

Wettability of a solid surface is an important property [29] because controlling the surface wettability is crucial in many practical applications in MEMS and biomaterials etc. [30, 31].

1.2.1.1 Wenzel model of wetting of rough surfaces

If a droplet of liquid is placed on a solid surface, the solid–air and liquid–air interfaces come together under the static or most stable CA (contact angle), θ_y (Figure 1.5 (a)). The value of θ_y can be determined from the condition of the total free energy

of the system being minimized and is given by the so-called Young–Dupre equation for the CA showed in equation (1) [32, 33].

$$\cos \theta_y = \frac{\gamma_{SA} - \gamma_{SL}}{\gamma_{LA}} \dots\dots\dots(1)$$

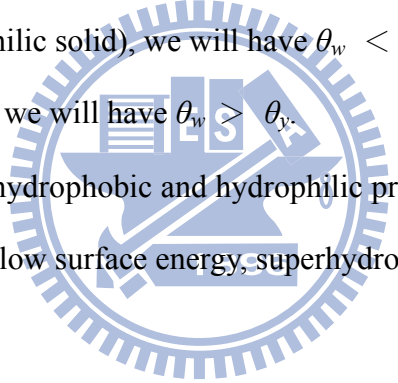
Where γ_{IJ} designates the surface tension (or energy) between phase I and J (S: solid, A: air and L: liquid). For a rough solid surface that consists of asperities and valleys with a typical size of roughness details smaller than the size of the droplet (Figure 1.5 (b)), the CA θ_w was calculated by Wenzel [34] as:

$$\cos \theta_w = r \cos \theta_y \dots\dots\dots(2)$$

Where, $r = A_{SL}/A_F$ is a roughness factor defined as a ratio of the solid–liquid area A_{SL} to its projection on a flat plane, A_F . Wenzel’s relation embodies two types of behavior:

1. If $\theta_y < 90^\circ$ (hydrophilic solid), we will have $\theta_w < \theta_y$ since $r > 1$.
2. Likewise, if $\theta_y > 90^\circ$, we will have $\theta_w > \theta_y$.

Thus roughness magnifies hydrophobic and hydrophilic properties of a surface and by roughening a material with low surface energy, superhydrophobicity can be achieved.



1.2.1.2 Cassie-Baxter model of wetting of rough surfaces

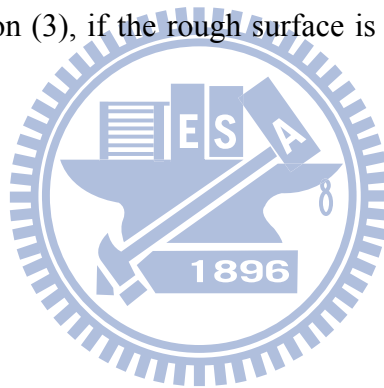
For a rough surface, a composite solid–liquid–air interface may form air pockets at the valleys between asperities with the flat fractional geometrical area of the solid–liquid and solid–air interfaces under the droplet f and $1 - f$, respectively (Figure 1.5 (c)). Transition to the composite interface increases CA and dramatically decreases solid–liquid contact area, and therefore decreases adhesion of liquid to solid, allowing the droplet to roll easily along the solid surface. Cassie and Baxter [35] found that for fractional solid–liquid and solid–air interfaces, the CA is given by [32, 33]

$$\cos \theta_c = r f \cos \theta_y - 1 + f \dots\dots\dots(3)$$

Equation (2) may now be considered a special case of Equation (3) with $f=1$ (no air under the droplet). For a heterogeneous interface consisting of two fractions with the CAs θ_1 and θ_2 , and the fractional areas f_1 and f_2 (so that $f_1 + f_2 = 1$), the Cassie and Baxter equation has the form:

$$\cos\theta_c = f_1\cos\theta_1 + f_2\cos\theta_2 \dots\dots\dots(4)$$

Equation (4) is reduced to Equation (3) in the limiting case of $\cos\theta_1 = -1$ (corresponding to the contact with air pockets, with $\theta_1 = 180^\circ$), $\theta_2 = \theta_y$, $f_2 = f$, and $r = 1$ (e.g. flat-top surface). The opposite limiting case of $\cos\theta_1 = 1$ corresponding to $\theta_1 = 0^\circ$ (water-on-water contact) yields $\cos\theta_c = 1 + f(\cos\theta_y - 1)$. This form of the Cassie-Baxter equation is used sometimes for the homogeneous interface instead of Equation (3), if the rough surface is covered by holes filled with water.



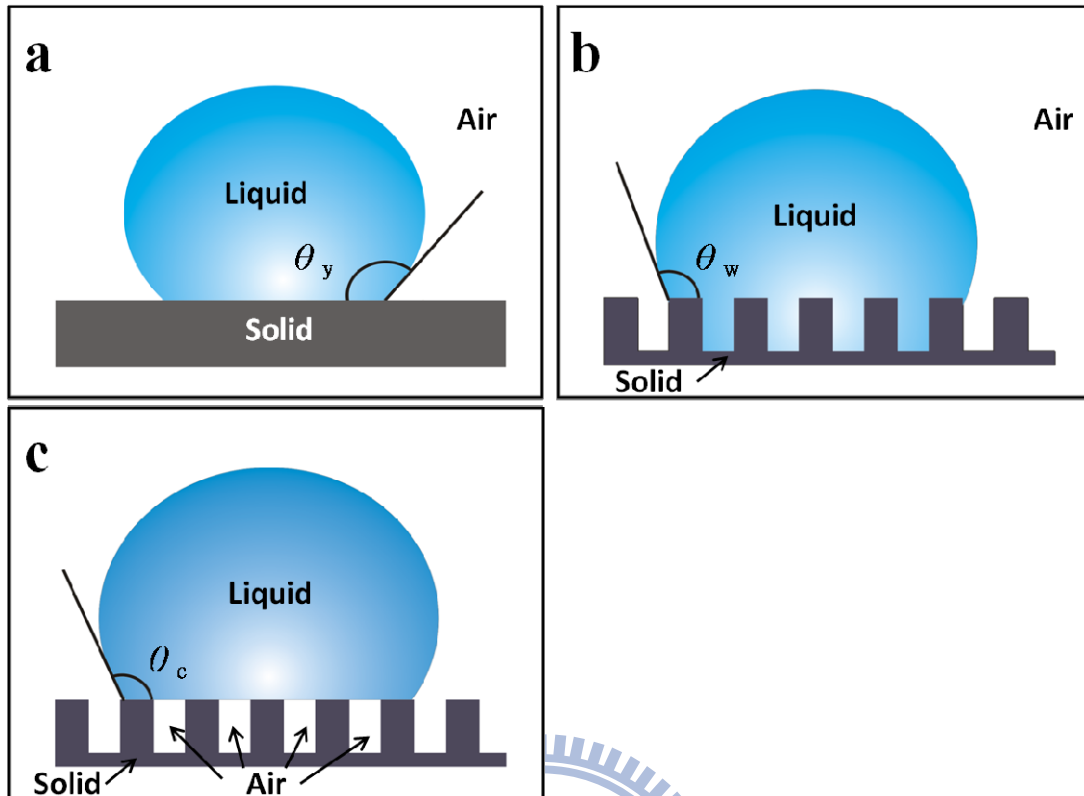


Figure 1.5 A liquid droplet in contact with (a) a smooth solid surface (b), (c) a rough solid surface. (b) Illustrate Wenzel's wetting state. (c) Illustrate Cassie's wetting state.

1.2.2 Lotus effect-a superhydrophobic and self-cleaning surface

Lotus leaves are one of the most famous examples among naturally occurring superhydrophobic surfaces [22]. The water contact angle (CA) of a lotus leaf is $161 \pm 2.7^\circ$ with CA hysteresis of 2° [36]. Pictures of a lotus leaf and its microstructure image obtained by Barthlott are shown in Figure 1.6 [37]. The structure of a lotus leaf consists of a combination of a two scale roughness: one around $10 \mu\text{m}$ (rough structure) and one around 100nm (fine structure). These surfaces are also referred as hierarchical micro- and nano-structures [4, 5]. The hydrophobicity of a lotus leaf arises from the epicuticular wax secreted by the leaf itself [27]. The wax has a contact angle of 110° , not highly hydrophobic; however, the lotus leaf still exhibits a superhydrophobic property. It is presumed that this combination of roughness and

wax contribute to the superhydrophobicity of the lotus leaf [4, 26]. The rolling off of water droplets and collecting the contaminants from the lotus leaf is dubbed as the “lotus effect”. The lotus leaf therefore always exhibits a very low degree of contamination: self-cleaning. The hierarchical structured surface of the lotus leaf provides a model for the development of biomimetic self-cleaning surfaces. On these water-repellent surfaces, water droplets move easily at a low inclination of the leaf and collect dirt particles adhering to the leaf surface [38].



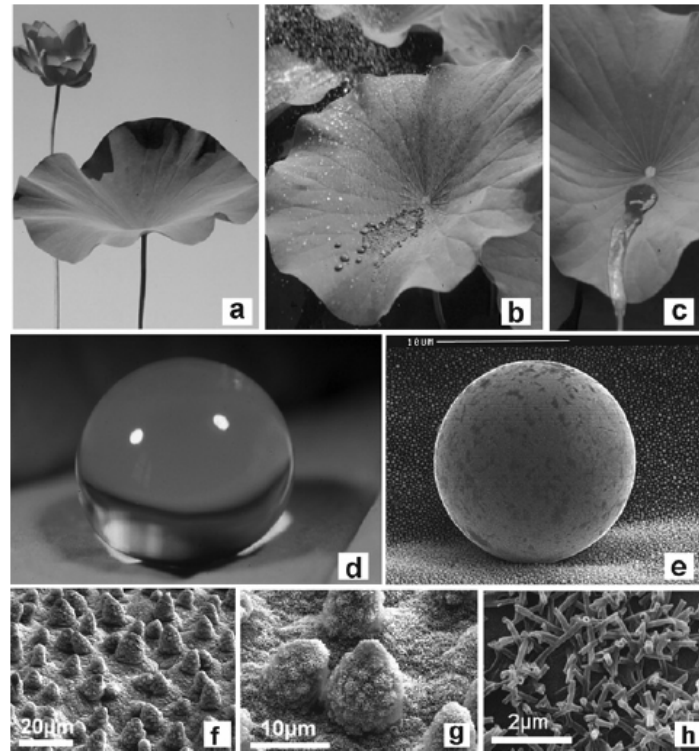


Figure 1.6 Superhydrophobic and self-cleaning surfaces. A flowering plant of Lotus (*Nelumbo nucifera*) is shown in (a). A Lotus leaf contaminated with clay (b) and removal of the adhering particles by water (c). (d) A spherical water droplet on a superhydrophobic leaf is shown. (e) SEM micrograph of a droplet illustrates the low wettability of superhydrophobic microstructured surfaces. The SEM micrographs show the Lotus leaf surface in different magnifications: (f) randomly distributed cell papilla, (g) a detail of the cell papilla and (h) the epicuticular wax tubules on the cells are shown.

1.2.3 Petal effect-a superhydrophobic and high adhesive surface

Hierarchical micropapillae and nanofolds are known to exist on the petals' surfaces of red roses (Figure 1.7 [39]). These micro- and nano-structures provide a sufficient roughness for superhydrophobicity and yet at the same time a high adhesive force with water. A water droplet on the surface of the petal appears spherical in shape, which cannot roll off even when the petal is turned upside down. Jiang et al. define

this phenomenon as the “petal effect” as compared with the popular “lotus effect” [39]. From the point of practical applications, this surface will be more useful in the synthesis of chemical engineering materials and microfluidic devices [40].

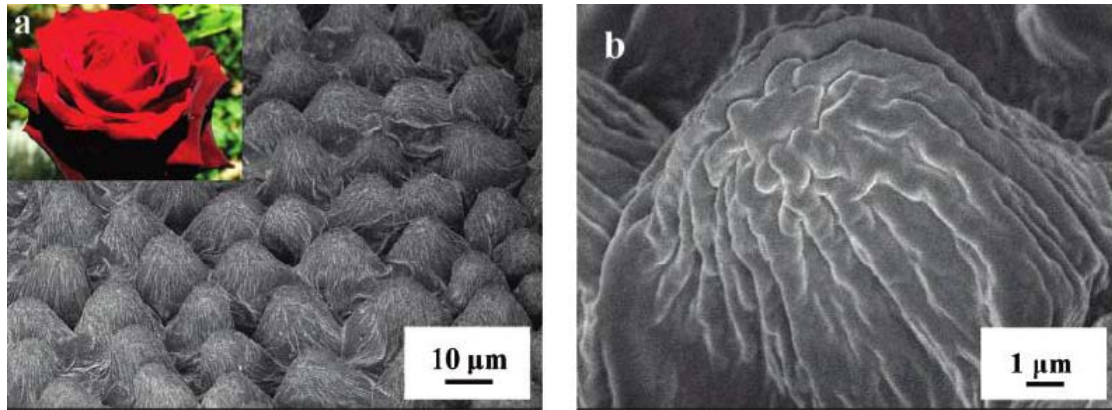
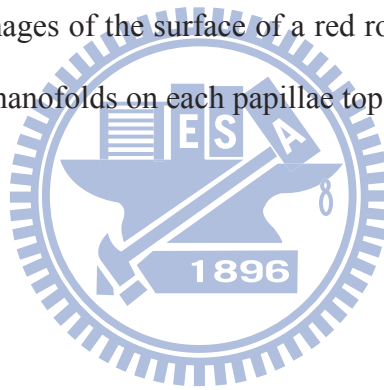


Figure 1.7 (a), (b) SEM images of the surface of a red rose petal, showing a periodic array of micropapillae and nanofolds on each papillae top.



Chapter 2: Literatures Review

2.1 Superhydrophobic surfaces with high adhesive force for water

Superhydrophobic surfaces with different dynamic wettabilities, such as water repellent or water adhesive, have attracted increasing interest recently [1-8]. The lotus leaf, with ultrahigh water contact angle (CA) and low sliding angle (SA), is widely known as a model superhydrophobic surface because of its self-cleaning property. Although superhydrophobic surfaces with high SA cannot be self-cleaning, they have many other potential applications, such as in the field of microfluidic control systems [9-15]. Superhydrophobic surfaces that can “pin” liquid droplets have been demonstrated for no-loss microdroplet transfer or trace-liquid reactors [16-22]. The ability of adhesive force to liquid is caused by van der Waals’ force and capillary force. It is known that superhydrophobicity is effective for obtaining a small liquid interfacial contact area (ICA), at least for water-based liquids, which significantly reduces the mass loss in microdroplet transfer [23, 24]. Here the common surface of superhydrophobicity and water adhesion can be divided into four types: hairy-type, tube-type, convex-type and other type.

2.1.1 Hairy-type structure

In Nature, beetles, flies, spiders and geckos have evolved their prodigious clinging ability that enables them to attach or detach from surfaces efficiently [25, 26]. Especially, the gecko, which has been the main focus of scientific researches, is capable of producing high adhesion force because of the hierarchically assembled, hairy structures found on its foot.

The biomimetic methods for fabricating functional surfaces with good

superhydrophobicity and highly water adhesion are inspired from gecko's foot. The strategy to fabricate the gecko-mimetic hairy structure was based on replica molding using an anodic aluminum oxide (AAO) template. Replica molding, one of soft lithographic techniques, is an efficient replication method, and has been applied for micro/nanofabrication. The technique enables highly complex structures in a mold to be truly replicated into multiple copies with nanometer resolution in a simple, reliable, and inexpensive way. The results for the formation of the gecko-mimetic nanopillar films are shown in Figure 2.1 [27]. The different tilt angles of water are presented in Figure 2.2 [27].

The hydrophobicity of the gecko-mimetic, nanopillar structured surface was ascribed to the air trapped between *h*-PDMS nanopillars. The trapped air can prevent the intrusion of water into the nanostructures, resulting in increase of the water contact angle on the nanostructured *h*-PDMS surface. This explanation could be confirmed by the Cassie–Baxter regime. The strong adhesion between polar water and non-polar *h*-PDMS nanostructures can be explained mainly by the dispersive adhesion caused by van der Waals' forces [28].

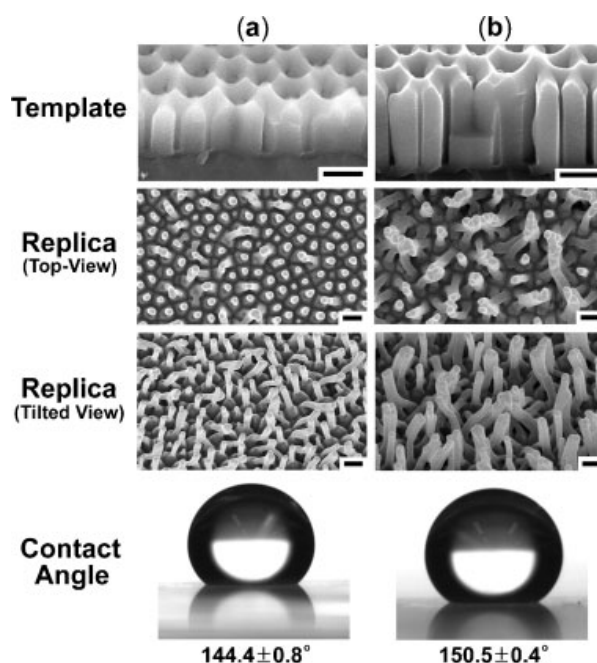


Figure 2.1 FE-SEM images of AAO templates anodized at the second anodization for (a) 10 min and (b) 20 min, and their *h*-PDMS replicas. The bottom shows a static water contact angle on the each replica surface. The scale bar is 500 nm.

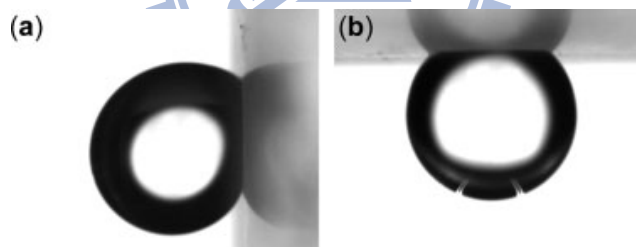


Figure 2.2 Shapes of a water droplet on the fabricated, hairy *h*-PDMS nanopillar surface with different tilt angles: (a) 90° and (b) 180°.

Dressick et al. have introduced a bottom-up process based on oblique angle deposition as a simple, robust method for controlling the morphology of poly-(*p*-xylylene) (PPX) films. They fabricated superhydrophobic films through the chemisorptions of fluoroalkylsiloxane coatings to hydroxyl sites created on the PPX film surface and controlled both water wettability and adhesion through appropriate

choices of PPX surface chemistry and roughness. Figure 2.3 [29] showed the film's structure and the ability to pin a water droplet on the fabricated surface. These results suggested that van der Waals and/or capillary forces sufficient to induce wetting behavior associated with the intermediate state are present for the structured PPX films [29].

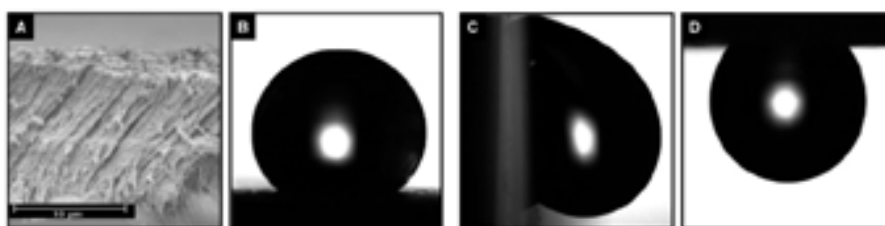


Figure 2.3 (a) Cross-sectional SEM image of the structured PPX-COCF₃ film. Shapes of water droplets on the structured PPX-COCF₃ film with different tilt angles: (b) 0°, (c) 90°, and (d) 180°.

2.1.2 Tube-type structure

A capillary lithographic approach was demonstrated by Jiang et al. [30]. An alumina membrane was used as the mold for the preparation of aligned polystyrene (PS) nanotubes. The PS solution was cast on glass and the membrane was then brought into contact with the PS cast. After capillary molding, the membrane was dissolved in NaOH and aligned PS nanotubes were obtained. The PS nanotubes showed a contact angle of $162 \pm 1.7^\circ$. The authors concluded that the water droplet was in a composite state (the Cassie–Baxter regime). However, it was found that the water droplet does not roll off the surface even at tilted angle of 180° (Figure 2.4 [30]), indicating that the surface is very sticky, although superhydrophobic. The authors have attributed this super sticky effect to the van der Waals' forces between the water molecules and the high density nanotubes generating a strong adhesion just like the

gecko's mechanism [31]. The authors have applied such a sticky surface as a mechanical hand to transfer a water droplet.

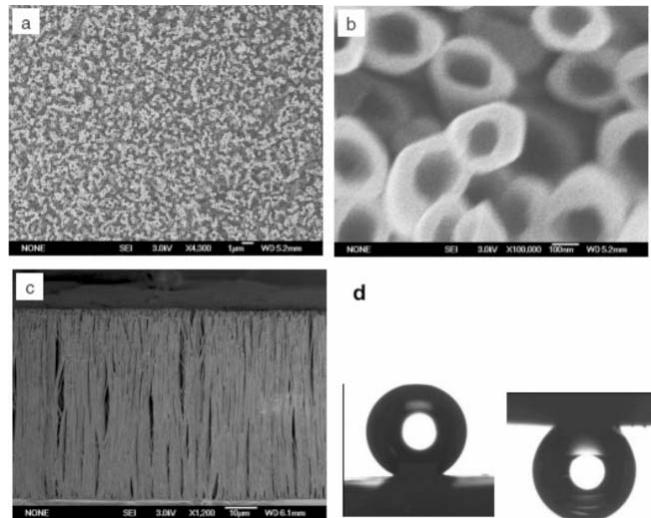


Figure 2.4 SEM images of PS nanotubes of (a) top view, (b) magnified image of (a), (c) side view and (d) the contact angle behavior.

Gao et al. [32] designed a nanotube array (NTA) based on basic principles of roughness-enhanced hydrophobicity and capillary-induced adhesion. The nanostructures were prepared with the simple electrochemical anodizing of pure Ti sheets. Then treated with a methanolic solution of hydrolyzed 1H, 1H, 2H, 2H-perfluorooctyltriethoxysilane (TEOS). The surface adhesive force may be effectively tuned by solid-liquid contact ways and the fractions of air pockets in open and sealed systems, which depend on the nanostructure configurations. In addition, authors found that the water adhesive force of the superhydrophobic NTA nanostructure surface could be tuned with changing the diameter of nanotubes and also the length of nanotubes, which was ascribed to the negative pressure [33] changes caused by the volume changes of the air, sealed in the nanotubes. These findings in Figure 2.5 [32] are very helpful in furthering the understanding of

superhydrophobicity, and also in guiding the design of new functional nanomaterials with custom-tailored surface hydrophobicity and adhesion [33].

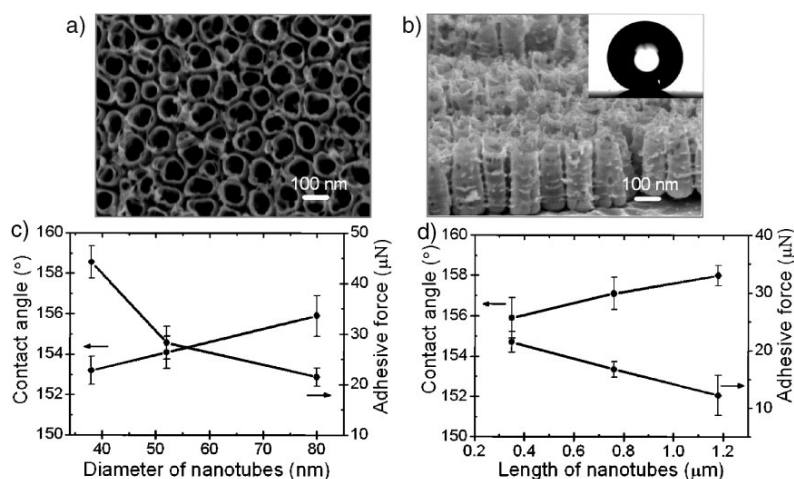


Figure 2.5 (a), (b) Top-view and side-view SEM images of superhydrophobic TiO₂ NTA nanostructures. The inset is a photo of a water droplet on the superhydrophobic NTA surface with diameters of 78 ± 14 nm. (c), (d) The curves of water contact angles and adhesive force on the superhydrophobic NTA nanostructures with respect to the diameter and length of nanotubes.

2.1.3 Convex-type structure

Huang et al. studied the dimension of the arrayed PDMS microlens for optimizing the hydrophobicity and adhesive force. The authors coated a positive photoresist (PR) on a silicon wafer then undergone the three dimensional (3D) diffuser lithography to patterned a surface consisting of dense arrays of micro-fabricated PDMS lenses. The micro lenses were showed in Figure 2.6 [34]. Afterward, the adhesive forces and contact angles were measured under different morphologies, showed in Figure 2.7 [34]. A perfectly ordered microlens array geometrically and crucially influences the hydrophobic behavior of the surfaces. Furthermore, the diameter and height of the microlens are crucial parameters that

govern the hydrophobicity. The wetting state belonged to the Wenzel model in which the droplet is able to wet the surface, thus resulting in a high-contact-angle hysteresis. The microlens arrayed surface thus becomes “sticky”.

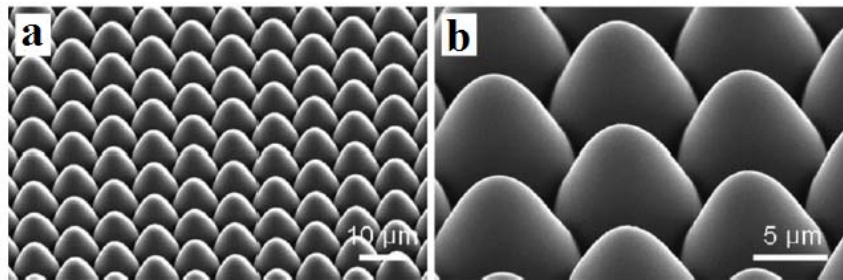


Figure 2.6 (a), (b) The microlens-arrayed surface morphology was apparent at high magnification.

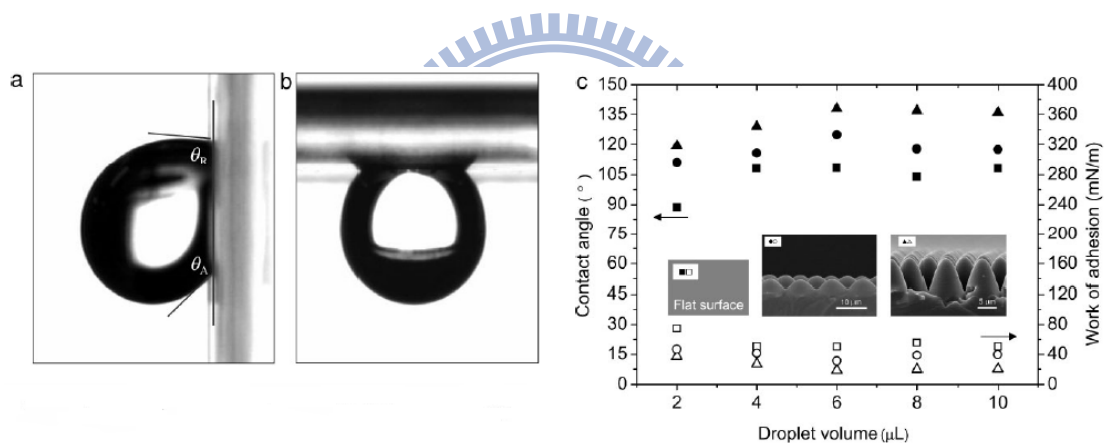


Figure 2.7 The adhesive force of a microlens array. (a), (b) Behavior of a water droplet on a 10×6 microlens-arrayed surface with tilt angles of 90° and 180° , respectively. (c) The work of adhesion (open symbol) and contact angle (solid symbol) as a function of the drop volume on the PDMS with flat surface (square), 10×2 array (circle), and 10×6 array (triangle). The work of adhesion was obtained directly from the contact-angle measurements. The insets show a cross-sectional view of the SEM images of the microlens array with different heights.

Jiang et al. used flash rose petals as a mold to duplicate the micro- and

nano-structure. The fabricated polystyrene (PS) surfaces which have morphology like rose petals' surface exhibited superhydrophobicity and high water adhesion as shown in Figure 2.8 [35]. The high adhesive force of the replica can be explained according to the Wenzel model. As illustration in Figure 2.9 [35], the water droplet can be pinned on the surface, because of the strong capillary force of the cone-shaped microstructures, which can force the water into the grooves of the surface. Therefore, the resulting replica shows superhydrophobicity with high adhesive force.

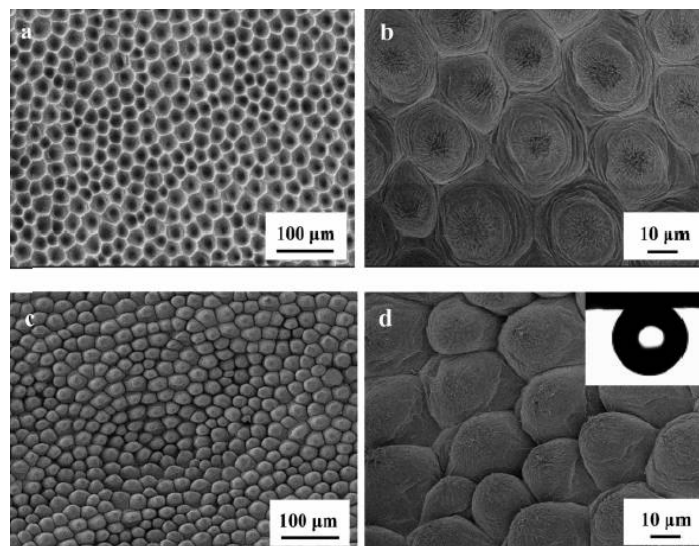


Figure 2.8 (a), (b) SEM images of the duplicated PVA film with inverse petal structures. (c), (d) SEM images of the duplicated PS film with the similar petal's surface structures. (Inset in panel d is the shape of a water drop on the PS film when it is turned upside down, indicating its superhydrophobic adhesive property.)



Figure 2.9 The water could permeate into the grooves of the surface. A droplet of water could pin on the replicated surface because of strong capillary forces.

Pogreb et al. fabricated the surfaces which had high apparent contact angles accompanied by high adhesion of water droplets similar to the rose petal. The surface was prepared by spreading lycopodium particles on the extruded polyethylene film and hot pressed with a crimped template. The topography and adhesive forces to water were shown in Figure 2.10 [36] and Figure 2.11 [36], respectively. This observation resembles the petal effect reported by Jiang et al. It is reasonable to relate the high adhesion of the droplets to the Wenzel wetting regime occurring on the lycopodium.

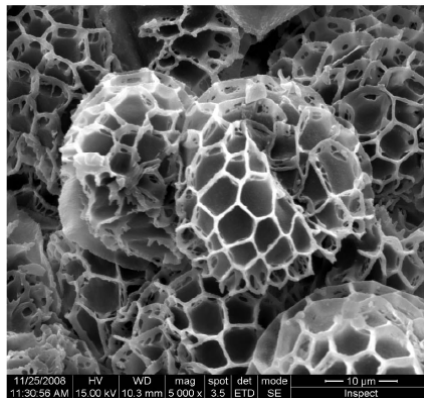


Figure 2.10 SEM image of the lycopodium-based substrate. The lycopodium particles were spread uniformly, the particles' sizes were quite similar about 30 μm in diameter, and the minimal pore size was 5 μm .

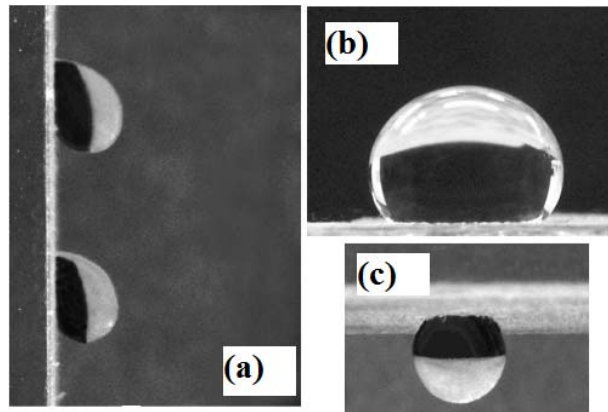


Figure 2.11 Water droplets (10 μL) attached to vertical (a) and horizontal (c) lycopodium-based surfaces. (b) Water droplet (40 μL) deposited on the lycopodium-based surface.

2.1.4 Other type structure

Besides the three types structures we mentioned above, other type structure with properties of superhydrophobicity and high adhesive forces toward a droplet of water can be found in nature, for instance, directional adhesion on the superhydrophobic wings of a butterfly (*Morpho aega*). A water droplet can easily roll off the surface of the wings along the radial outward (RO) direction of the central axis of the body, but is tightly pinned in the opposite direction. Interestingly, these two distinct states can be tuned by controlling the posture of the wings (downward or upward) and the direction of airflow across the surface (along or against the RO direction). When the wing is tilted upward, the flexible nanotip and microscales take a close arrangement. The water droplet is in the “wet” contact with the nanostrips and forms a quasi-continuous TCL, which pins it on the surface [37]. Figure 2.12 [38] showed properties of a water droplet on the superhydrophobic wings of a butterfly [38].

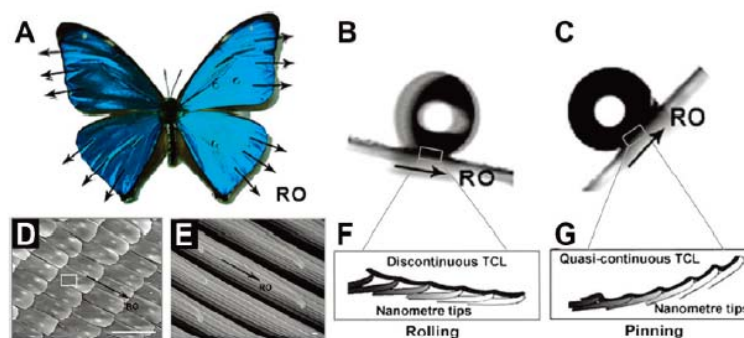


Figure 2.12 Directional adhesion on superhydrophobic butterfly wings and SEM images of the wings: (a) an iridescent blue butterfly (*Morpho aega*); the black arrows denote the RO direction away from the body's center axis; (b) the droplet easily rolls along the RO direction when the wing is tilted toward downward by 9° ; (c) the droplet pinned on the wing that is tilted upward; (d) (e) SEM images of the wings (scale bars = (d) $100\ \mu\text{m}$ and (e) $100\ \text{nm}$). (f), (g) Two models proposed for the potential mechanism of distinct adhesions (f) rolling state and (g) pinning state.

2.2 Motivation

Since Barthlott discovered that lotus leaf has the unusual anti-wetting property resulted from the special two scales topographies, micro- and nanostructure, scientists have been interested in the field of superhydrophobic surface with the ability of self-cleaning called "Lotus effect". Owing to the characteristic of lotus leaf, scientists craved to discover another useful functionality from variety of plants' surface. Recently, the superhydrophobic and highly adhesive property in a rose petal has been found which is entirely different from lotus leaf and called "Petal effect". Scientists, recently, have been fascinated by the sticky surface with superhydrophobicity. Herein, the micro- and nanostructures upon a rose petal inspired us to mimic the petal-like surface. We wanted to fabricate the topography by a simple bottom-up procedure because the complicated two scales structures were very difficult to achieve by a

top-down method. By using this way, it would bring us a low-cost and large-area fabrication in industrial process. Here we expected our petal-like surface possessed better features and performances, both superhydrophobicity and high water adhesion, than a nature petal. If the surface could be manufactured, we firmly believed that it's a new generational material that could be widely used in many fields, for instance, biomaterials, water-transform for a microsample analysis and design of micro-fluidic devices. Moreover, the design of our procedure even provided us to study micro- and nano-structures toward wetting characteristic, respectively.



Chapter 3: Experimental Section

3.1 General Introduction

All the experiments were preceded in National Chiao Tung University (NCTU). All the equipments were also conducted in our laboratories in NCTU. The reagents were purchased commercially and used by following with the directions unless specially mentioned.

All the reagents were listed alphabetically in the form of “Name {abbreviation; chemical formula; purity; manufacturer}”. Some information will be omitted if not available or not necessary. The following text will use the abbreviation of the reagent.

Deionized and distilled water {DI water, ddH₂O}

The water we used was purified with filters, reverse osmosis, and deionized system until the resistance was more than $18 \text{ M}\Omega \cdot \text{cm}^{-1}$. DI water was used to clean and wash.

Hydrogen peroxide {H₂O₂; ≥30%; Sigma}

Hydrogen peroxide was mixed with sulfuric acid to form piranha solution which cleaned the wafer surface.

Sulfuric acid {H₂SO₄; 98%; Sigma}

Sulfuric acid was mixed with hydrogen peroxide in a 3:1 ratio to remove impurities on the wafer surface. On the other hand, we mixed it with nitric acid for corrosion. This solution was very corrosive and dangerous. We must handle it with carefulness and patience.

Ethanol {C₂H₅OH; 99%; Sigma}

In this study, it was used for washing and dehydration of a fresh petal.

Nitric acid {HNO₃; 60-61%; Showa}

It was mixed with sulfuric acid for corrosion.

Polydimethylsiloxane {PDMS (Sylgard 184); Dow Corning}

We used PDMS to manufacture the superhydrophobic structure which was similar to petal's surface.

Poly (vinyl alcohol) {PVA; 87-89% hydrolyzed, high molecular weight (88,000-97,000; Alfa}

In this study it was prepared as a negative mold, micro-scale structure.

Polystyrene latex microsphere {PS; 35 μm in diameter; Alfa}

We dropped the latex solution on a silicon wafer to form a two dimension close-packed PS beads. The prepared film was to mimic the micro-scale part of a rose's petal.

Phosphoric acid {H₃PO₄; 5%; J. T. Baker}

Phosphoric acid was used to prepare a buffer in the fresh rose's petal dehydration.

Osmium tetroxide {OsO₄, 99.8%; Alfa}

Osmic acid was used to maintain the shape of a plant sample.

Glutaraldehyde {CH₂(CH₂CHO)₂; 25%; MP Biomedicals Inc.}

It was mixture with other solution to maintain the shape of a plant sample.

Paraformaldehyde {OH(CH₂O)_nH (n = 8 - 100); powder,95%; Sigma}

It was mixture with other solution to maintain the shape of a plant sample.

Sodium phosphate dodecahydrate {Na₃PO₄ • 12H₂O, 97%; Alfa}

The solution was prepared as a buffer solution during the dehydration process.

3.2 Flat PDMS with periodic wrinkles

The flat PDMS was prepared by mixing silicone base (reagent A) and curing agent (reagent B) in a weight ratio of 10:1. After degassing, the mixture was heated at 80°C for one hour. The final PDMS, which had the size of 1 cm² in area and 0.1 cm in thickness, was fixed on a wafer chip. Then flat PDMS on the wafer chip was immersed in a sulfuric acid solution, made of sulfuric acid/nitric acid in different volume ratio), for several seconds. After acid corrosion, it was immediately putted into a cold bath around 0°C for thirty seconds. The final step was drying the sample by nitrogen gas then vacuumed over night. Figure 3.1 illustrated the process for preparing the surface.

3.3 Petal-like PDMS surface manufacture

Experimental protocols to mimic the petal-like PDMS surface were schematized in Figure 3.2. First of all, the 2.5 wt% PS beads, which had 35 μm in diameter, were spread on a clean wafer chip treated with O₂ plasma. It was dried in barometric pressure until the total water was vaporization. Then the two-dimensional close-packed PS beads were formed owing to the water vaporization. Thereupon, we spread a 15 wt% PVA solution on the sample. A PVA-PS film was peeled from the wafer when the PVA solution was dried at atmosphere pressure. The film we received was slightly polished by using sandpaper. Afterwards, it immersed in an acetone solution accompanied with ultrasonic's bath until the PS beads were removed. Then the treated PVA film, replicated from the cross-packed PS beads, was used as a negative mold. PDMS, which had the same conditions as we mentioned in section 3.2, was spread on the PVA film. The next step was to degas for the purpose that avoid an air bobble in PDMS. When the PDMS was dried, we peeled it off and fixed it onto a clean wafer. Finally, the PDMS undergone an acid corrosion process as same as we

mentioned in section 3.2.

3.4 Fresh rose petal and chrysanthemum petal dehydration

Firstly, the fresh rose's petal was sliced up into many part, each chip had a size of 0.5 cm². The chip of petal was immersed in the 0.1 M solution, composed of a phosphate buffer solution had a pH value equal to 7.0, a 2 wt% glutaraldehyde solution and a 4 wt% paraformaldehyde solution, for 2 hours. The prepared petal was then immersed in the 0.1 M solution consisted of a phosphate buffer solution had a pH value equal to 7.0 and a 2 wt% osmium tetroxide solution for 2 hours. Subsequently, the treated petal was washed by the phosphate buffer solution for many times. Afterward, the cleaned petal was processed through a dehydration process by using a series of alcohol solution, it had a concentration of 20%, 30%, 50%, 70%, 80%, 90% and 100% respectively. The treated sample was submerged by each alcohol solution for 20 minutes and then immersed in an acetone solution for 20 minutes. It shall be repeated three times before migrating to next high concentration alcohol solution. Finished the dehydration process, the almost dried sample had to undergo a critical point dry by a carbon dioxide liquid ensured total water was removed from the petal.

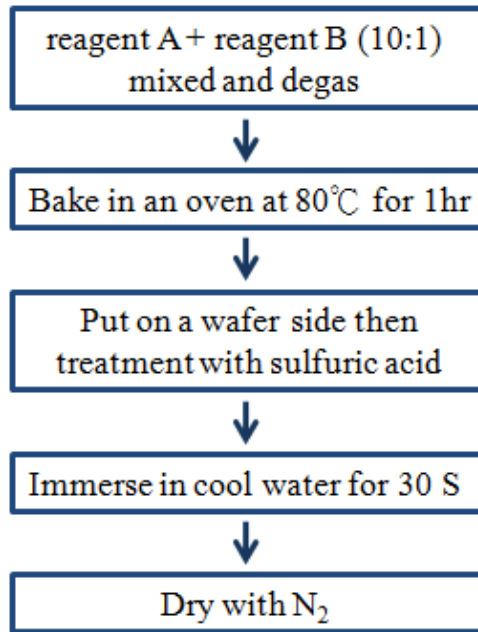


Figure 3.1 The flow chart of preparing the superhydrophobic PDMS surface.

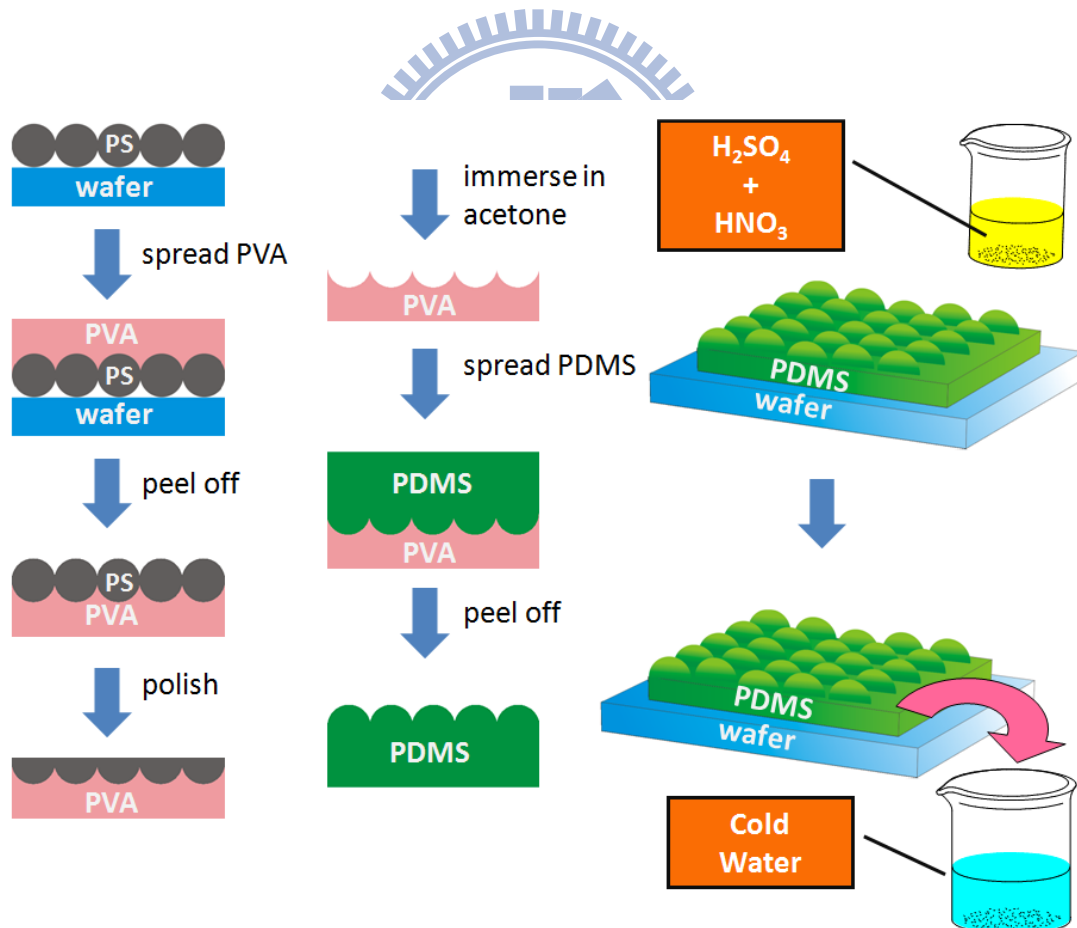


Figure 3.2 The scheme showed the protocol of manufacturing a petal-like PDMS.

3.5 Specimen characterization

(A) SEM

SEM is a very useful tool for observing surface morphology of specimen. SEM has secondary electrons or backscattered electrons detectors passing the signal to computer and forming image. In this study, the micro- or nanostructure of the prepared PDMS, close-packed PS beads on wafer and duplicated PVA film were all characterized by a field-emission scanning electron microscopy (FE-SEM, JEOL-6700) operating at 10 kV accelerating voltage.

(B) FT-IR

The position of Fourier transform infrared spectrometer (FT-IR) as a useful technique for characterization of polymeric materials has been firmly established last decades. FT-IR has brought additional merits such as high sensitivity, high precision, quickness of measurement, and extensive data processing capability besides the intrinsic advantages of infrared spectroscopy such as wide applicability, nondestructiveness, measurement under ambient atmosphere, capability of providing detailed structural information, and a huge data base. We prepared the specimen by scrapping the treated surface then mixture the bits and small pieces with potassium bromide powder. After that, we grinded the mixtures to a small size as possible as we could. Finally, pressed the mixtures to a chip. The chip was then characterization by FT-IR (Nicolet Avatar 320).

(C) Inverted light microscopy

Light microscopy is widely used to observe a biological specimen. Upright light microscopy and inverted light microscopy are the most popular equipment for characterization transparent samples. In this study, we used an inverted light microscopy (Olympus CKX41) to characterize the periodic wrinkles on a PDMS surface.

(D) Contact angle meter

A measurement of a static contact angle is a general method to understand the wetting phenomena of a surface. A surface with a static contact angle larger than 150 degree is regard as a superhydrophobic surface. Herein, we investigated the anti-wetting properties of the resulting surfaces by using a contact angle meter (FTA175). The average contact angle was from five different position measurements on the same surface.



Chapter 4: Results and Discussion

4.1 The results of periodic wrinkles on plane PDMS

After the flat PDMS being treated by the corrosive acid, it immediately took a cold bath for several seconds. The resulting surface exhibited regular periodic wrinkles whose periodicities were in a micro-scale. A reasonable explanation was the thermal contraction of an underlying substrate; we would show more details below.

4.1.1 Surface topography

A flat PDMS was treated by a strong acid composed of sulfuric acid and nitric acid with several reaction conditions as listing in table 4.1. The resulting surfaces were examined by an inverted microscope; the photographs were showed in Figure 4.1 and Figure 4.2. We could find the randomly orientation of wrinkles, but it reveal a regular periodicity. Figure 4.1 (a)-(d) showed the periodicities ranging from 4.31 μm to 26.27 μm according to different immersion times of 5 s, 15 s, 30 s, and 60 s, respectively. Another experimental condition was illustrated in Figure 4.2 (a)-(d). The treated surfaces with periodicities ranged from 26.28 μm to 109.86 μm under appropriate immersion time of 5 s, 15 s, 30 s, 60 s, respectively. We joined these results together and showed in Figure 4.3. We concluded that the periodicity increases with the increase of immersion time and the sulfuric acid volume percentage in the mixture acid. Furthermore, we also investigated the relationship between reaction temperature and the resulting periodicity. The results in Figure 4.4 revealed that there was only slightly increase of periodicity with the increase of reaction temperature. The temperature increased from 20°C to 50°C lead to a slightly increase of periodicity which increased from 8.6 μm to 14.22 μm . Herein, we got an experience that we

could increase the periodicity by modulating the concentration of sulfuric acid in the mixture acid and reaction temperature. After examining the microstructure, we used SEM to obtain the nanostructure as shown in Figure 4.5. The nanostructure on the wrinkle would lead to a superhydrophobicity as the property of lotus leave, as shown in Figure 4.5 (b)-(d).

time \ ratio	S/N = 1/1	S/N = 2/1
5 s	#1	#5
15 s	#2	#6
30 s	#3	#7
60 s	#4	#8

Table 4.1 The reaction conditions were listed above, in which, S/N presented the volume ratio of sulfuric acid over nitric acid, #1~#8 represented serious samples' numbers, first column indicated the reaction time, all the samples reaction at 55°C; after acid corrosion, samples was cooled by a cold water for 30 seconds at 2°C~3°C.

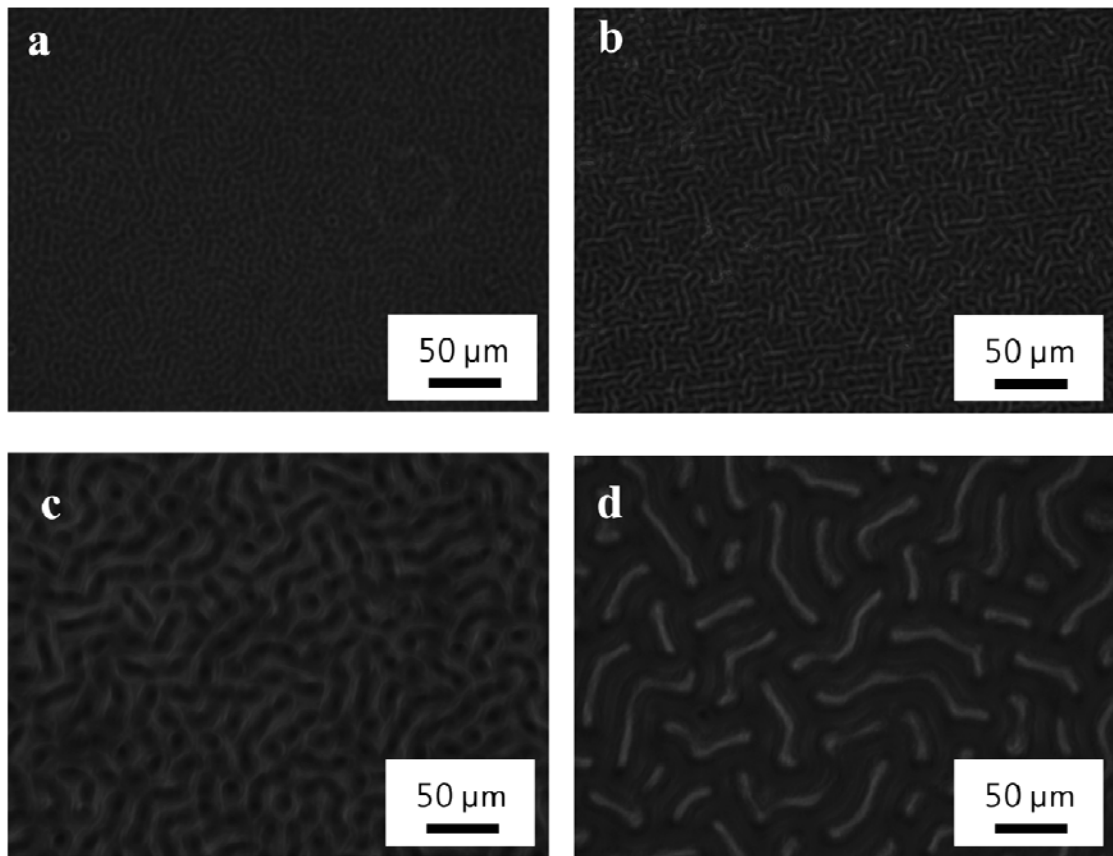


Figure 4.1 Optical microscopy images of the PDMS going through acid, mixture of sulfuric acid and nitric acid under the 1/1 volume ratio, corrosion with different treatment times of (a) 5 s, (b) 15 s, (c) 30 s, and (d) 60 s.

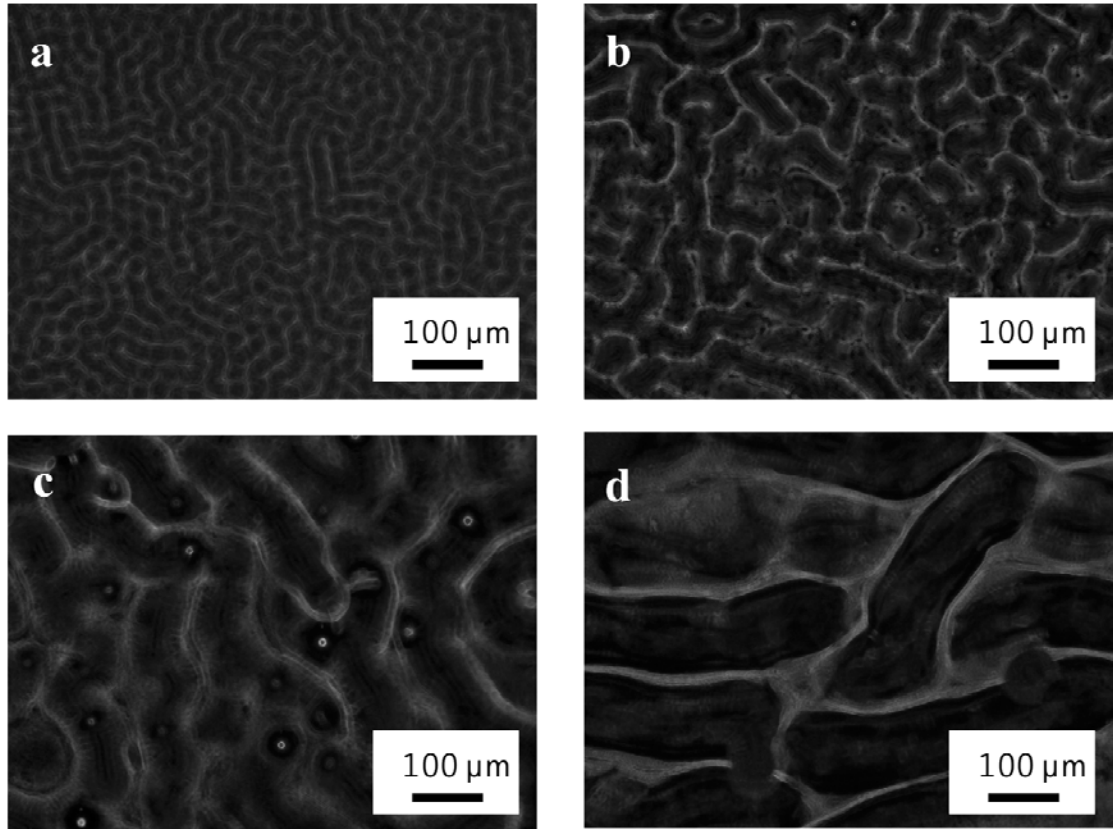


Figure 4.2 Optical microscopy images of the PDMS going through acid, mixture of sulfuric acid and nitric acid under the 2/1 volume ratio, corrosion with different treatment times of (a) 5 s, (b) 15 s, (c) 30 s, and (d) 60 s.

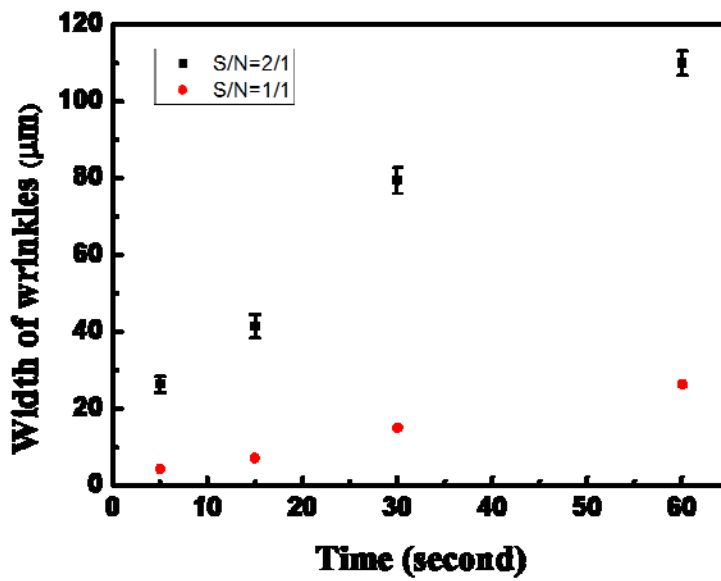


Figure 4.3 Scheme showed the periodic wrinkles resulted from the increasing immersion time at different acid composition of sulfuric acid/nitric acid = 1/1 and 2/1 in volume ratio.

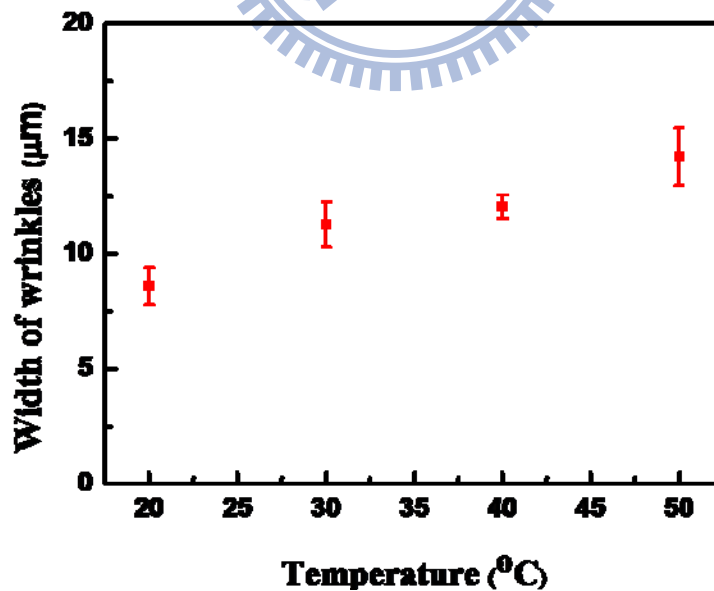


Figure 4.4 The scheme indicated that width of the periodic wrinkles at the same corrosion time was proportional to the reaction temperature. The acid was composed of sulfuric acid and nitric acid in a volume ratio of 1/1.

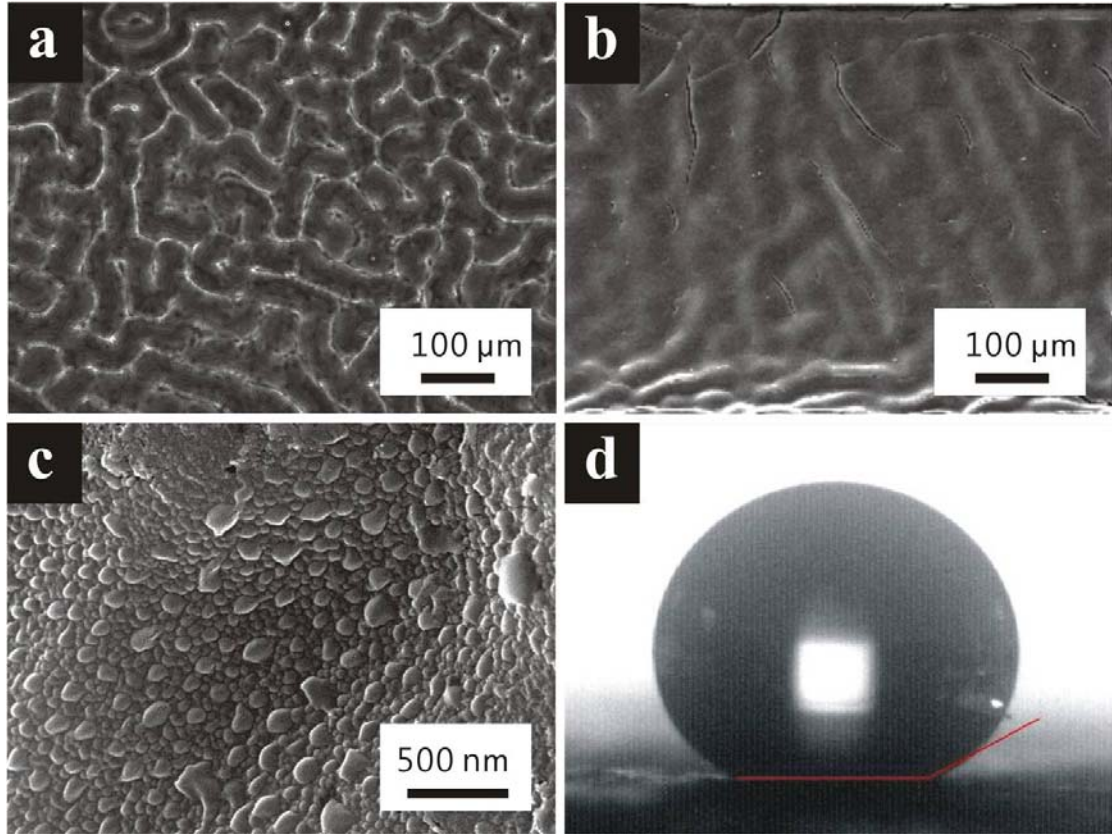


Figure 4.5 The PDMS treated with acid producing a superhydrophobic and non-sticky surface. (a) Optical microscope image of periodic wrinkles PDMS caused by acid corrosion. (b), (c) SEM images showing two scales, micro- and nano-, structures. (d) A 5 mg water droplet located on the superhydrophobic and non-sticky PDMS surface, showing a contact angle of 151.5° .

4.1.2 Mechanism of resulting periodic wrinkles

The spontaneous formation mechanism of periodic wrinkles of double layers systems have been studied by many scientists, for instance, metal/soft-polymer film [1]; moreover, PDMS surface treated by O_2 plasma could produce the similar results. In our experiment, the flat PDMS was fixed onto a silicon waver; the top of PDMS was corrosion by acid. It generated double layers; one was the upper layer PDMS, reacted with acid solution, the other was under layer PDMS. The upper layer was called modified layer or stiff layer; on the other hand, the under layer was the bulk of

PDMS which still maintained flexibility. The differences of thermal-expansion coefficient and the Young's modulus between modified layer and under layer soft PDMS led to a compressive stress. When cooling process, the periodic wrinkles were formed owing to the releasing compressive stress. Figure 4.6 revealed the formation mechanism of the periodic wrinkles. As our study above, the compress stress σ (Pa) could be given by equation (5) [2]:

$$\sigma = \frac{E_m(\alpha_p - \alpha_m)(T_0 - T_1)}{1 - \nu_m} \dots\dots\dots(5)$$

where E_m (Pa) and ν_m (unitless) are the Young's modulus and Poisson's ratio of the modified layer, α_p ($^{\circ}\text{C}^{-1}$) and α_m ($^{\circ}\text{C}^{-1}$) are the thermal-expansion coefficients of PDMS (under layer) and modified layer, respectively, T_0 and T_1 are the sample temperature and the temperature when the system is stress free. The periodicity L (m) when the wrinkles formation under the double layer system could be express by equation (6) [2]:

$$L \approx 4.36t \left(\frac{E_m(1 - \nu_p^2)}{E_p(1 - \nu_m^2)} \right)^{1/3} \dots\dots\dots(6)$$

where t is the thickness of modified layer, E_m (Pa) and ν_m (unitless) are the Young's modulus and Poisson's ratio of the modified layer, E_p (Pa) and ν_p (unitless) are the Young's modulus and Poisson's ratio of the PDMS (under layer).

As discussions we mentioned above, to modulate the volume percentage of sulfuric acid in the mixture acid and reaction time, thickness of the modified layer would be changed which caused the formation of periodic wrinkles. Herein, we could conclude that the periodicity was proportional to the volume percentage of sulfuric acid and immersion time, because of the increase of modified layer. By the equations (5) and (6), they might be not correct under real situation but would be credible and applicable in our double layer system; the conjectures tally with the results from

section 4.1.1. Moreover, the acid corrosion resulted not only the periodic wrinkle but also the nanoscale convex with the width under 100 nanometer. In the acid corrosion experiment, it was hard to find the periodic wrinkle when the sulfuric acid/nitric acid ratio less than 1/1 because of insufficient sulfuric acid to produce effectively modified layer. Furthermore, when we substantially increased the immersion time, more than 2 minutes, wrinkles would be merged; the periodicity could not be observed.

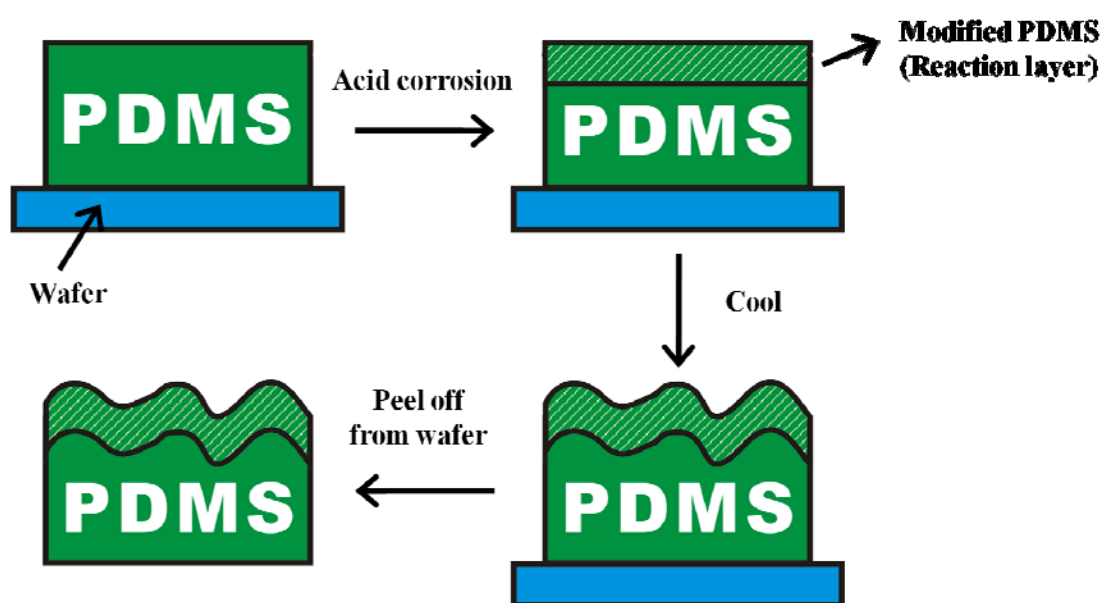


Figure 4.6 The formation mechanism of periodic wrinkles under a flat PDMS. A flat PDMS was fixed onto a clean wafer then undergone an acid corrosion. Outer layer of PDMS was reacted by acid which caused a different thermal expansion coefficient between inner layer (bulk PDMS) and outer layer (Reaction region). During cooling process, it formed periodic wrinkles.

4.1.3 Chemical functional group analysis

PDMS (Sylgard 184, Dow Corning) we prepared was composed of two intergradient; one was pre-polymer that composed of about 60 repeating units of $-\text{OSi}(\text{CH}_3)_2-$ terminating with a vinyl $-\text{CH}=\text{CH}_2$ group, the other was curing agent

that was composed of about 10 repeating units of $-\text{OSi}(\text{CH}_3)_2-$ and silicon hydride $-\text{OSiHCH}_3-$. The curing step was shown in equation (7) [3]. We investigated the chemical structure of PDMS by FT-IR spectra. Table 4.2 listed expected FT-IR absorption band of chemical structures of pure PDMS and common groups. The FT-IR spectra we received was shown in Figure 4.7 which indicated the FT-IR spectra of pristine and acid corrosion PDMS respectively. The peak of 1260 cm^{-1} resulted from the Si-C chemical bond of $-\text{Si-CH}_3$ functional group; the peak of $1130\text{-}1000\text{ cm}^{-1}$ indicated the Si-O chemical bond of $-\text{Si-O-Si-}$ functional group; the peak of $2280\text{-}2080\text{ cm}^{-1}$ came from Si-H single bond; the peak of $2962\text{-}2960\text{ cm}^{-1}$ resulted from the C-H chemical bond of CH_3 functional group; the broad peak of $3700\text{-}3200\text{ cm}^{-1}$ resulted from the O-H chemical bond of $-\text{OH}$ functional group. In these points, we could conclude that in our system, there had no chemical structure changed when it under the stable stage after acid corrosion. On the other hand, the $-\text{OH}$ resulted from the acid remained or the small amount of penetration steam. Hence, the wetting phenomenon of superhydrophobicity was resulted from the sculptured topography by acid corrosion instead of chemical modifications of PDMS. The micro- and nano-structure, the two level structures were similar to lotus leave, would repel water to cause a high contact angle.

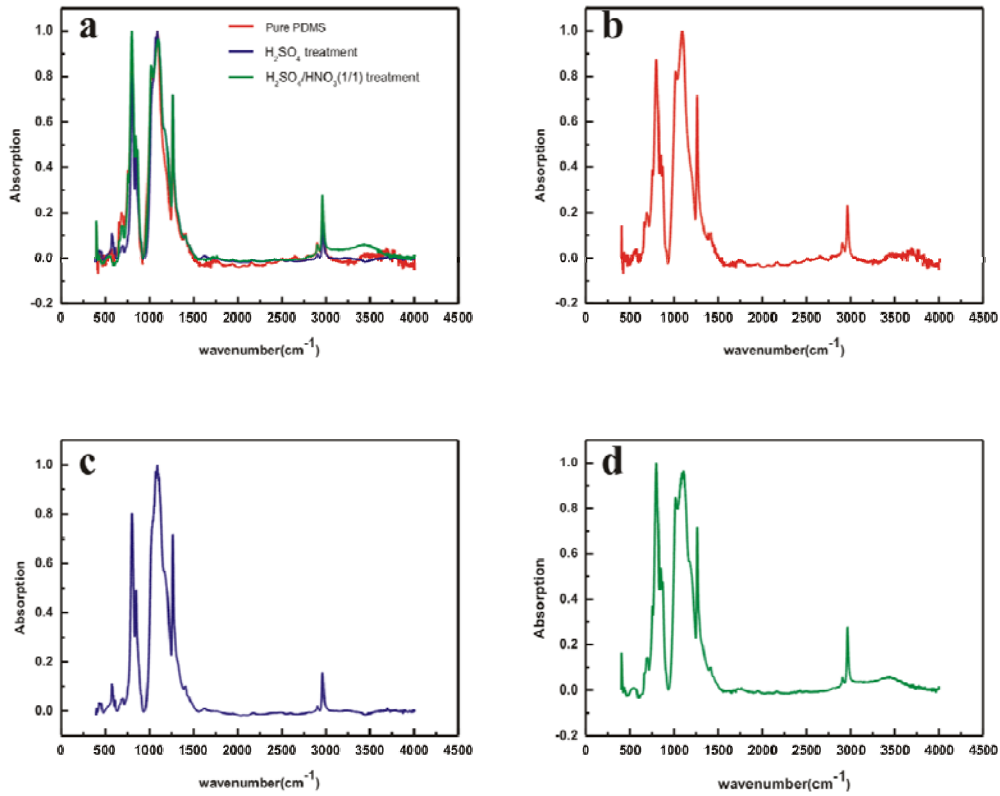


Figure 4.7 An scheme indicated the FT-IR spectra of PDMS surface (a) comparison (b), (c) and (d); (b) no treatment and (c) treated by pure sulfuric acid (d) treated by mixture acid, sulfuric acid/nitric acid = 1/1 in volume ratio.

4.1.4 Wetting phenomenon of the surface

According to our previous study, the anti-wetting property of modified PDMS was caused by the microstructure periodic wrinkles and raised nanostructure. There are two possible wetting states for the superhydrophobic PDMS: (1) Wenzel’s state, water attaches to the sculptured surface, and (2) Cassie’s state, water cannot penetrate to the sculptured surface and trap air inside. Equation (2) describes the Wenzel’s model [4]:

$$\cos\theta_w = r\cos\theta_y \dots\dots\dots(2)$$

where θ_w and θ_y are the Wenzel’s contact angle (the contact angle on the roughness surface) and Young’s contact angle (the contact angle on a flat surface) ,respectively

and r present the roughness factor, defined as the ratio of true surface area to the apparent surface area. The Cassie's model can be expressed by equation (3) [5]:

$$\cos\theta_c = r f \cos\theta_y - 1 + f \dots\dots\dots(3)$$

where θ_c and θ_y are the Cassie's contact angle (the contact angle on the roughness surface) and the Young's contact angle (the contact angle on a flat surface), respectively, r is the ratio of the actual area to the projected area of the solid surface that is wetted by the liquid, and f is the area fraction of the projected wet area. As our best knowledge, the high contact angle hysteresis would happen in Wenzel's state; on the other hand, Cassie's state could induce a low contact angle hysteresis, for instance, lotus leaf tend to exhibit Cassie's state. Herein, we concluded that superhydrophobicity of the modified PDMS surface resulted from Cassie's state because the surface we fabricated had a small sliding angle (lower than 5°).

Unlike carbon hydride polymer, PDMS consists of silicone base bone which caused a much resistant to environmental damage, for instance, resist corrosive acid or base solution. This advantage lead to it has the potential to application toward industrial field. For this reason, we prepared several corrosive solution, ranged from pH=1 to pH=14, to examine our modified PDMS. The results showed that the superhydrophobic property not only for pure water but also for corrosive solution. Figure 4.8 showed the high contact (around 150°) when a corrosive solution dropped on the modified PDMS surface. Moreover, we prepared more corrosive solution to obtain the results as shown in Figure 4.9. All the corrosive solution located on treated PDMS showed a high contact angle about 150°.

From the FT-IR spectra, there had no change of chemical structure. The fabricated PDMS just changed the topography, two level structures (micro- and nanostructure) as shown above. Hence, we offered another evidence to prove that the superhydrophobic property resulted from the change of topography not chemical

structure. Figure 4.10 showed the superhydrophobic property maintained with days go by. If superhydrophobicity caused from chemical modification, it would decrease with time increase; for instance, when PDMS treated by SF₆ plasma, the superhydrophobicity would decayed with time increase. Our results indicated that the sustained superhydrophobic property induced owing to the micro- and nanostructures of modified PDMS surface, it would be unconcerned with chemical modification.

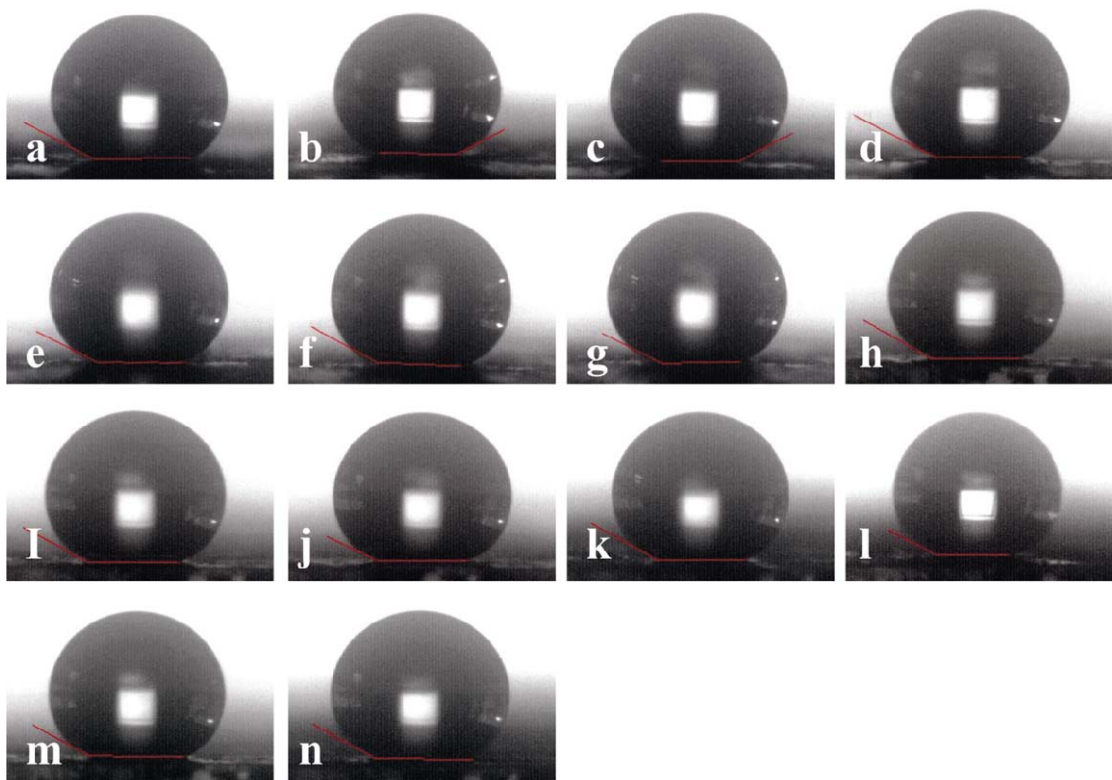


Figure 4.8 (a)-(n) Images showed the contact angle changed from different condition solution, pH values changed from 1-14. The superhydrophobic property of the treated PDMS surface maintained as similar as the pure water. A high contact angle around 150° was revealed during the wide range of pH values.

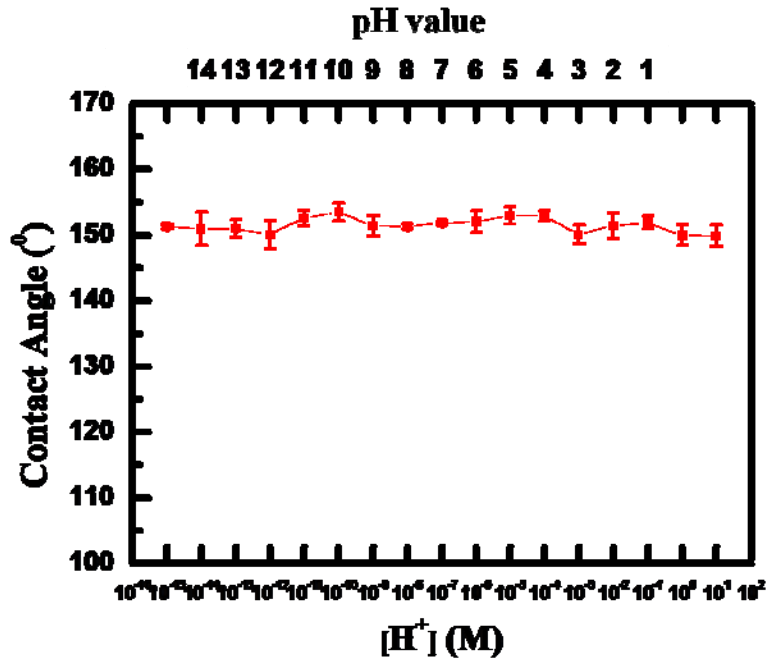


Figure 4.9 Images showed the wetting phenomena of different [H⁺] solutions.

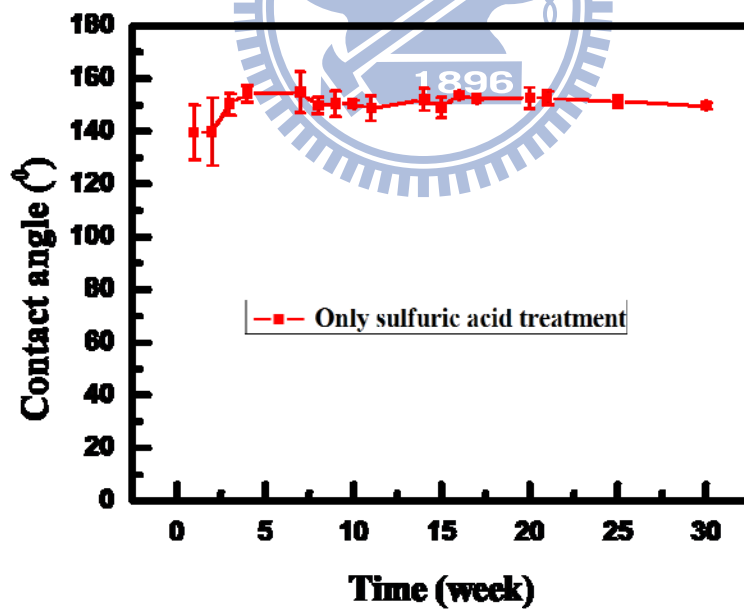


Figure 4.10 Graph showing the relationship between time and contact angle on the treated PDMS.

4.2 Petal-like surface characterization

After a raining day, a rose petal is shining because many small water droplets were spread on it even if a wind over blow the petal. Until the last, the unusual phenomena have been studied by scientists. The ability of water adhesion in a rose petal is very different from a lotus leaf in which a water droplet can easily roll off. Because of the two level scales of micro- and nanostructures, the rose petal exhibits a high adhesive force for a water droplet. The topographies of petals are shown in Figure 4.11. From the coevolution opinion, the micro-convex with nano-fold allow bees to grip flowers and increase foraging efficiency [6]. Herein, we attempted to fabricate a rose petal-like structure by a bottom up method, the results were showed later.



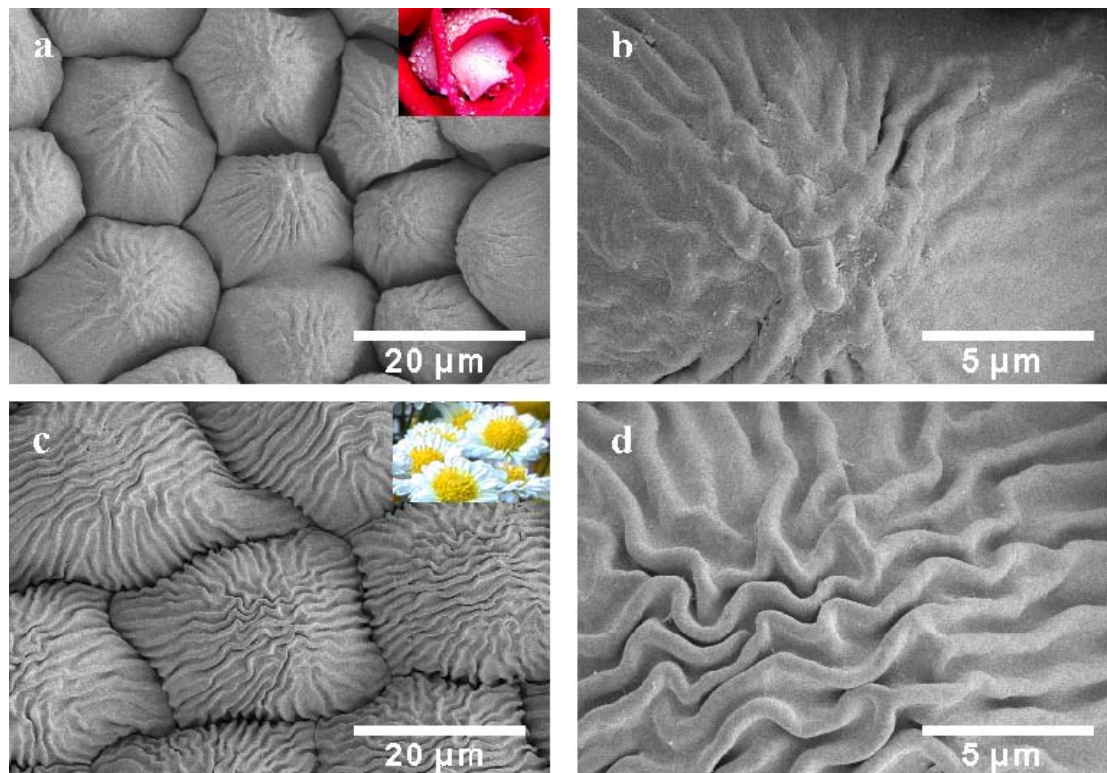


Figure 4.11 The SEM images of dehydrated (a), (b) a rose-petal and (c), (d) a chrysanthemum-petal, the surface showed the large-scaled convex and the nano-fold. The convex structure is about 20~30 μm in width and the nano-fold is less than 1 μm .

4.2.1 Three level structures analysis

The morphology of rose petal inspired us to fabricate a superhydrophobic surface with high water adhesion. Firstly, a two-dimensional, a monolayer, of polystyrene (PS) sphere was assembled on a silicon wafer owing to the attractive capillary forces and water flow caused by evaporation [7]. Figure 4.12 schemes the formation of the close-packed PS spheres. Then we manufactured micro-convex by using the close-packed PS spheres as a duplicated mold. In our experiment, the PDMS replica had the same topography of close-packed PS spheres and subsequently dipped in the prepared solution, the acid solution composed of sulfuric acid and nitric acid. We examined the treated PDMS by SEM as shown in Figure 4.13. There were three level

structures on our fabricated surface. The primary structure came from the replica of close-packed PS spheres had a convex about 30~35 μm in width, the decrease of radius was caused by replication process and acid corrosion. The secondary structure was the wrinkle had several hundreds of micrometer in width and the tertiary structure was the small convex with the width less than 100 nm. The nanoscale structures were resulted from the acid corrosion as we mentioned earlier toward the formation of wrinkles on a flat PDMS. Herein, we joined the three level structures as shown in Figure 4.14.

A flat surface is easy to form a wrinkle on it via banding; by contrast, it's very hard to produce a wrinkle from a spherical surface because the external stress will be released by the symmetrical sphere. As the phenomena we mentioned above, the wrinkles, produced from the double layer system, on the convex PDMS had smaller periodicity than on the flat one. For the reason above, we had to dip the PDMS for several times to ensure the formation of periodic wrinkles.

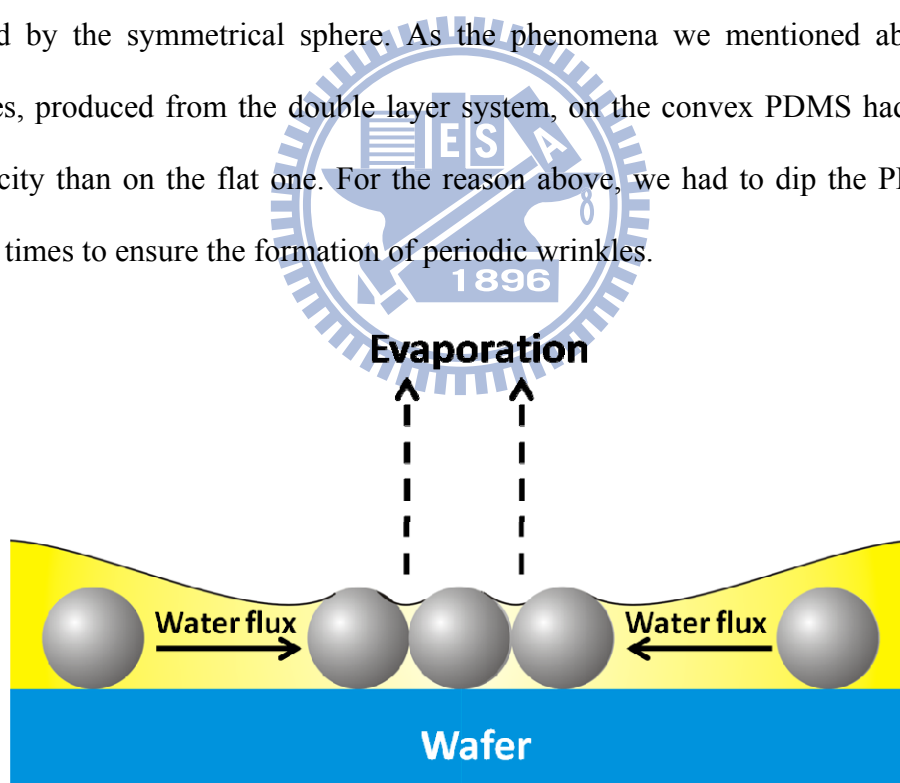


Figure 4.12 Scheme showed the formation of PS spheres assembled on a silicon wafer caused by the water flow.

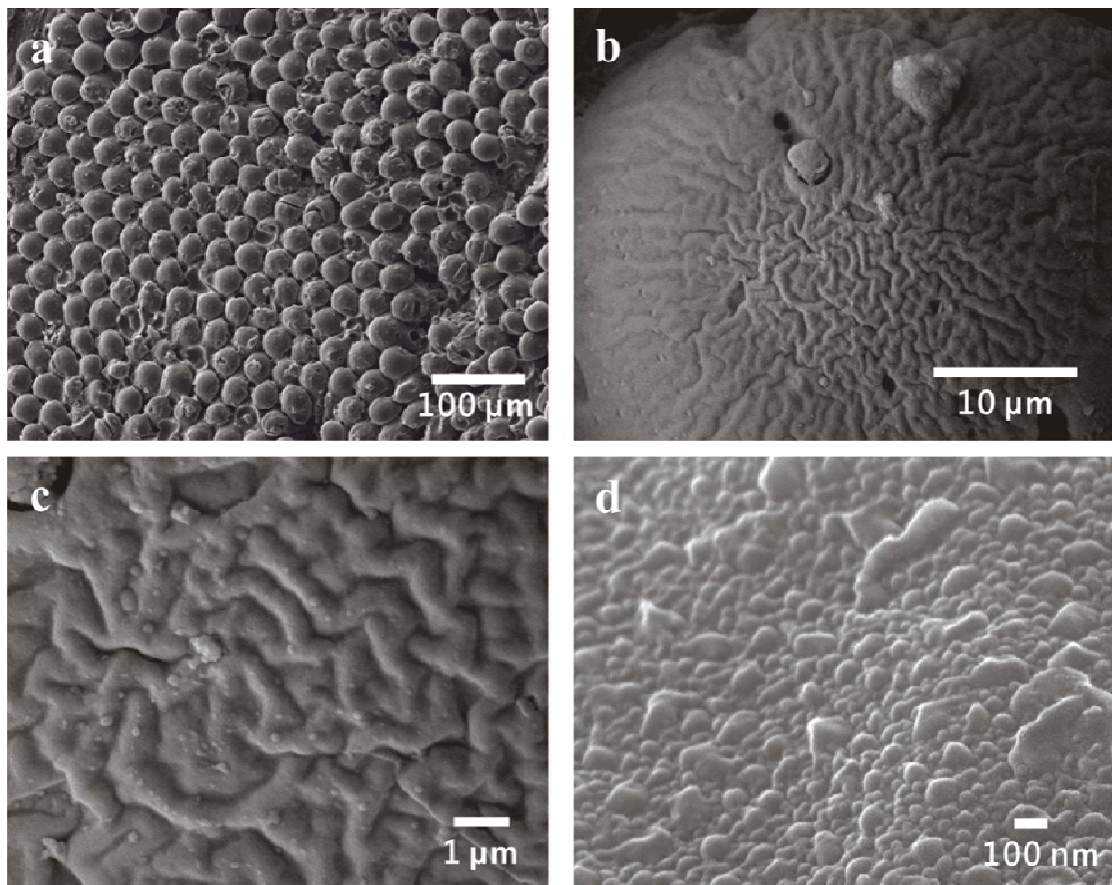


Figure 4.13 (a) The SEM image show the close-packed convex. (b), (c) Showing SEM images for the manufactured surface with the topography which was similar to the rose-petal (d) SEM image indicated the nanostructure of the surface.

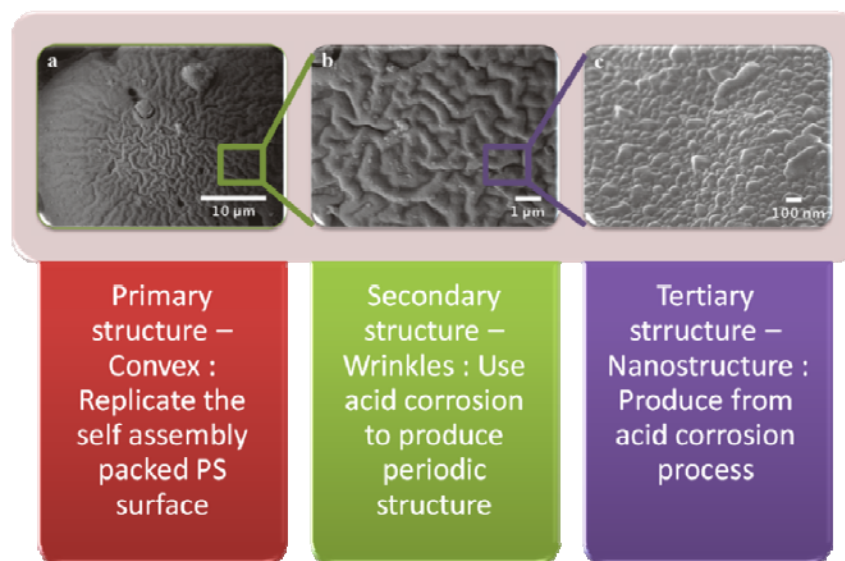


Figure 4.14 Scheme showed the three level structures on PDMS

4.2.2 Cassie impregnating wetting state

Figure 4.15 were the images of a water droplet on PDMS surface, encompassed three structures. To investigate the wetting phenomena, we prepared flat and convex PDMS to compare with the petal-like PDMS. Surface roughness magnifies the underlying properties; both hydrophilic and hydrophobic characteristics are reinforced by surface textures when the wetting property of Wenzel's state [8]. Because of the insufficient roughness, the formation of air pockets is impossible on the flat and convex PDMS. For this reason, when a water droplet deposits on the flat PDMS or that on the convex one, the wetting state will obey Wenzel's model. The petal-like PDMS was unlike the flat or convex PDMS; it had sufficient roughness for formation of air pockets underneath the water droplet. There, consequently, were two possible wetting states for our petal-like PDMS. One was Cassie's state that we have mentioned earlier, the other was Cassie impregnating state, in which, grooves of the solid are wetted with liquid and solid plateaus are dry [9]. The petal-like PDMS exhibited the high adhesion for water so the wetting state tended to the Cassie impregnating state instead of the Cassie's state. In the Cassie impregnating model, the water film can impregnate along with the topography; nevertheless, the water film even can wet the upper part of the surface, the bottom still dried. For water, the close-packed microscale convex was easy to penetrate, but the nanoscale structures could repel the water. Herein, a droplet of water placed on our fabricated PDMS spread on the surface and penetrated the depth of the support. The scheme was shown in Figure 4.16.

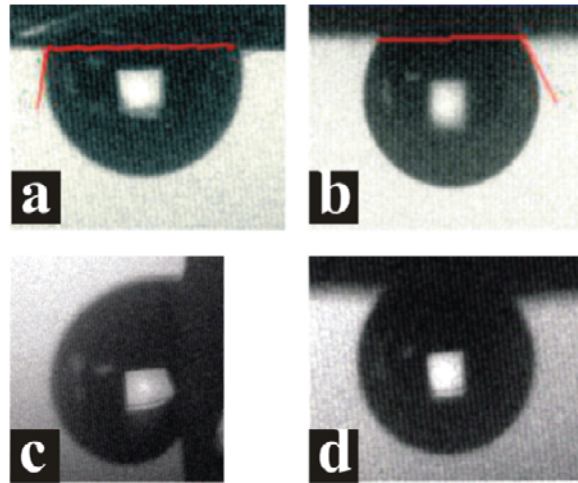


Figure 4.15 A 5 mg water droplet pinned on (a) a flat PDMS surface, (b) a PDMS with micro-scaled convex, and (c), (d) a PDMS surface with petal-like morphology when turning the surface vertically (90°) and upside (180°) respectively.

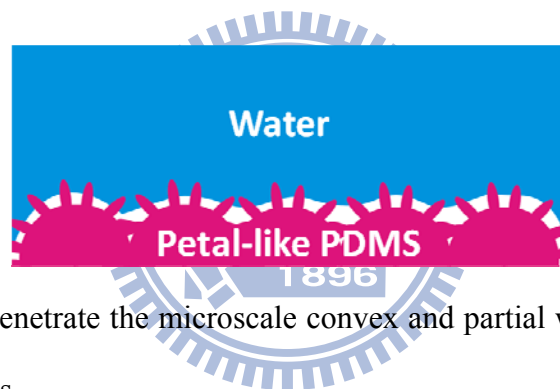


Figure 4.16 Water penetrate the microscale convex and partial wetting the upper part of nanoscale wrinkles.

4.2.3 High adhesive forces for water

In this section, we displayed the adhesive properties toward flat, convex, and petal-like PDMS. Moreover, we also showed the relationship between dipping times and adhesive forces. Figure 4.17 indicated that the adhesive forces and water contact angles received with different structures. With roughness increasing, the contact angles changed from 93.42° to 128.68° and 150.01° . A water droplet located on the flat and convex PDMS was revealed the Wenzel's wetting state because the two topographies had insufficient roughness to trapped air under the water. The different of contact angle between the flat and convex PDMS owing to the surface roughness.

On the other hand, air pockets could be obtained when a water droplet deposited on the petal-like PDMS. It's because of the formation of wrinkles and nanostructures after the acid treatment; the more air trapped, the more increase of water contact angle. The adhesive forces increased from 11.37 N/m², 14.48 N/m² to 35.81 N/m², the adhesive forces of the flat and convex PDMS were due to the van der Waals interactions between the liquid and solid supports. A theatrical adhesive force obtained from the petal-like PDMS was caused by van der Waals interaction and capillary force. As earlier study, the wetting state of petal-like PDMS is Cassie impregnating state; the water, hence, can penetrate to the grooves and the upper wrinkles. The extended contact area between the liquid and the solid support caused the larger van der Waals interaction than the flat and convex PDMS. Besides, the trapped air induced a large capillary force when the water droplet was going to pull out from the surface. According to the reasons above, the petal-like PDMS revealed a high adhesion for water. To investigate the induced adhesive forces from wrinkles and nanostructures, we measured the adhesive forces and contact angles of petal-like PDMS treated by several circumstances of dipping times. As showed in Figure 4.18, the dipping times from 3 to 4 and 5 caused the increases both adhesive forces and water contact angles. The water contact angles increased from 137.93°, 148.80° to 150.01° with dipping times increased from 3, 4 to 5, respectively. The three times dipping might induce slight wrinkles and nanostructures which could not increase sufficient roughness for trapping much air under the liquid; it, hence, showed the smallest contact angle and adhesive force. Under the dipping conditions of 4 and 5, the change of water contact angles and adhesive forces were small, less than 1% and 3%, respectively. The reasonable explanations of the increases were as follows. The longer acid treatment with time caused deeper wrinkles and more nanostructures which induced more contact area and much air trapping under the liquid, the van der

Waals interaction and capillary force were both increasing. These increases caused high water adhesion. However, too much acid treatment time, we could not obtain the petal-like PDMS because the formed wrinkles would be destroyed with the excess acid corrosion. We joined the results that PDMS with several morphologies in Table 4.3.

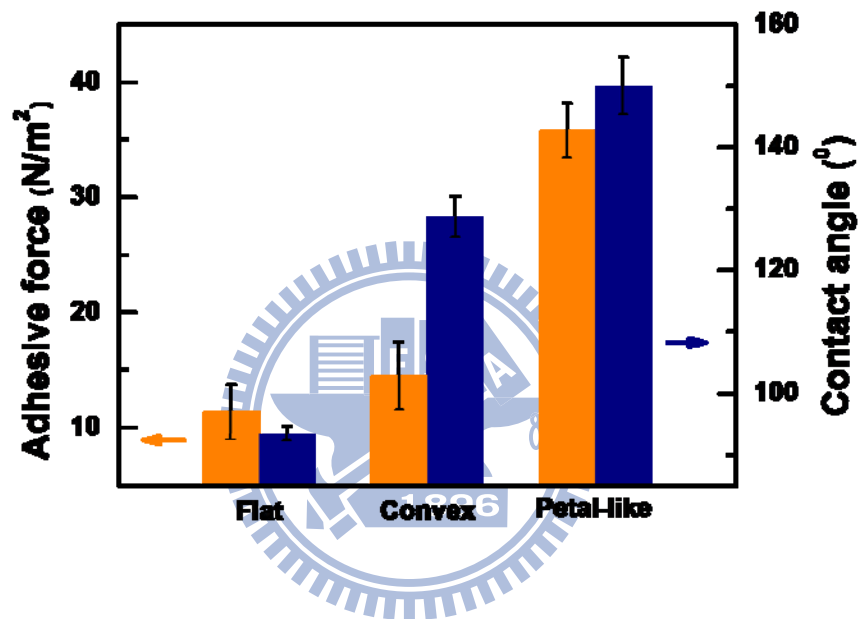


Figure 4.17 The graph of water contact angles and adhesive force between different morphology, flat, micro-scaled convex and petal-like topography.

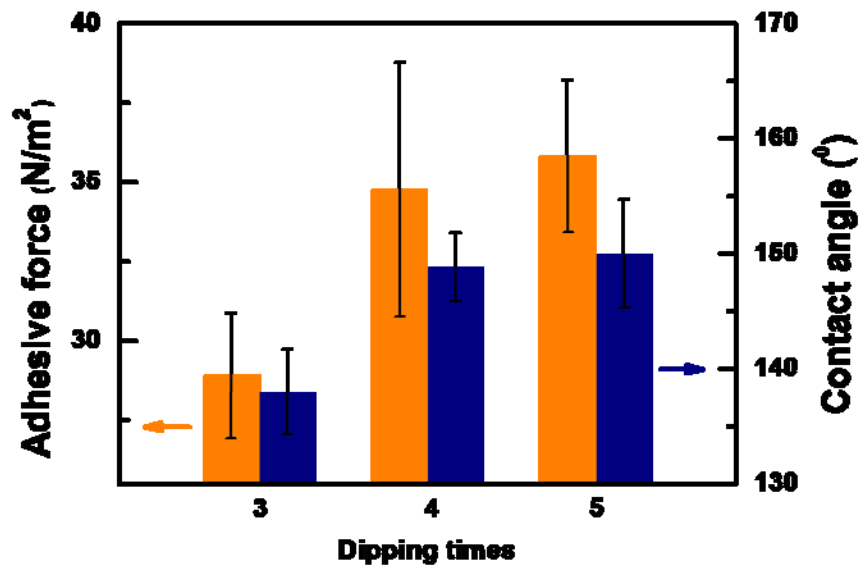


Figure 4.18 The histogram of water contact angles and adhesive forces on the petal-like surface changed with decanting times. Blue rectangles indicated that adhesive force increased from 28.89 N/m² to 35.81 N/m². Orange rectangles showed the contact angle changed from 137.93° to 150.01°.




	Structure	Property	Wetting state	Reason
PDMS	Flat	Hydrophobicity	Wenzel state	Van der Waals interaction
	Periodic wrinkles	1. Superhydrophobicity 2. Self-clean	Cassie state 	Lotus effect
	Convex shape	1. Hydrophobicity ↑ 2. Adhesion ↑	Wenzel state 	Van der Waals interaction
	Petal-like shape	1. Superhydrophobicity 2. Adhesion ↑↑	Cassie impregnating wetting state 	Petal effect

Table 4.3 The wetting properties of different structure levels.

4.3 Innovative application of petal-like surface

4.3.1 A sticky palm for water transportation

Firstly, a flat PDMS treated by acid corrosion that had self-cleaning property we mentioned earlier was used as the superhydrophobic surface. Afterward, we deposited a 5 mg water droplet on the superhydrophobic surface. When the petal-like PDMS contact the water droplet, it immediately adhered to the petal-like PDMS. The water droplet was then transferred from the petal-like surface to a hydrophilic silicon wafer as shown in Figure 4.17. It's simple and easy to release the water droplet from the petal-like PDMS to the silicon wafer. As mentioned previously, hairy type and tube type surfaces also have a high adhesion to water. However, excessive adhesion resulted from strong van der Waals force is disadvantageous to water-releasing, and thereby such structures are unsuitable for liquid transportation. As the results we obtained, the petal-like PDMS had the potential of water transportation; moreover, it might be used in micro-fluid field.

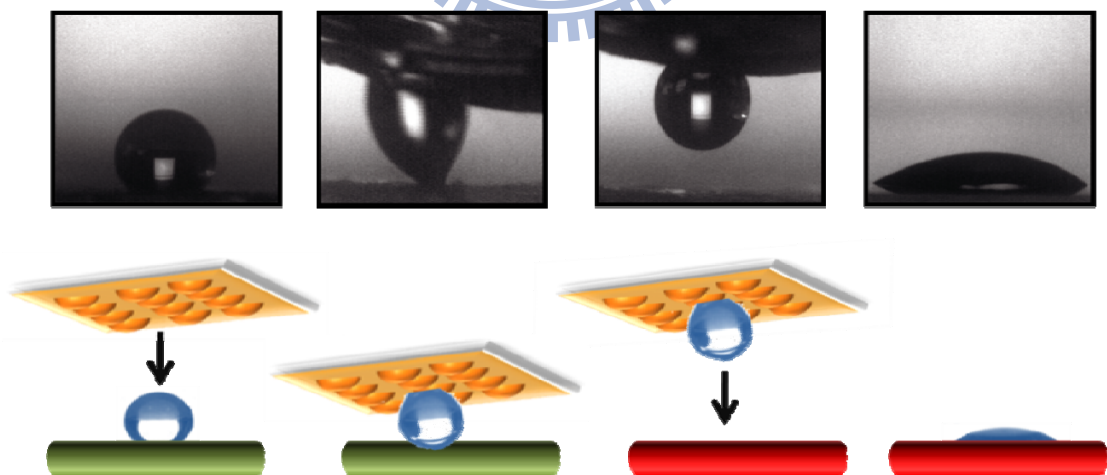


Figure 4.19 A 5 mg water droplet transported from a hydrophobic and non-sticky surface to a hydrophilic surface by the petal-like surface PDMS.

4.3.2 A nonresidual stamp for imprint technique

To fabricate the nonresidual PDMS stamp, we designed the two superhydrophobic regions on the PDMS. One is the superhydrophobic area with self-cleaning and the other is the superhydrophobic area with high water adhesion. First of all, the convex PDMS was manufactured by duplicating the close-packed PS beads. Afterward, the convex PDMS was etched by a carbon dioxide laser. The remained region still had convex upon PDMS; on the other hand, the topography of the etching area became flat. The prepared PDMS, then, treated by acid corrosion process we have mentioned above (Figure 4.20 (a)). Here, the resulting PDMS had two wetting states, Cassie impregnating wetting state and Cassie's wetting state. The petal-like area just like a sticky palm to adhere the dye then released it to a paper. By contrast, the flat region exhibited non-sticky property because of the micro-wrinkles and nanostructures. We used the PDMS to imprint for several thousand times. It revealed that the stamp still as cleaning as the beginning (Figure 4.20 (b) (c)). This nonresidual property means we need fewer dye and cleanless process in imprinting, which brings advancements of low cost and environmental friend.

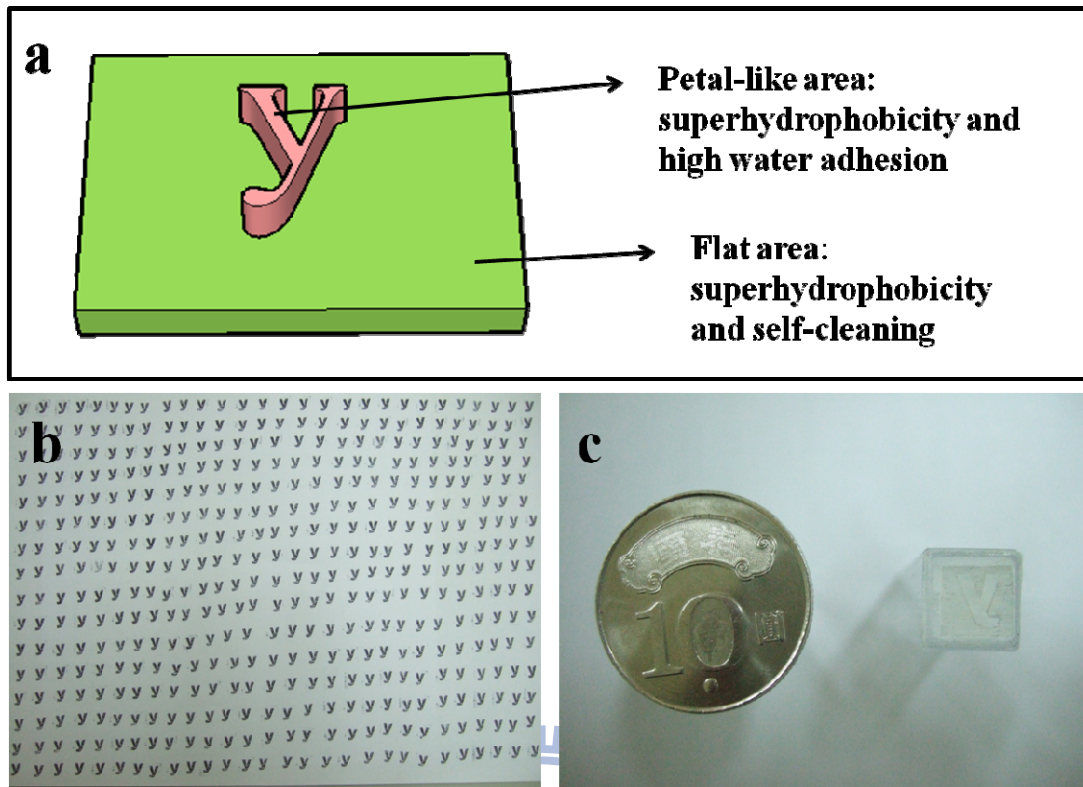


Figure 4.20 (a) Scheme indicated the two different superhydrophobic surfaces on the PDMS. (b) Several hundreds of patterns on the paper by using the fabricated PDMS stamp continuously. (c) The image showed the PDMS stamp remained cleaning after imprinting upon a paper with the stamp for several hundred times.

Chapter 5: Conclusion

A plane PDMS treated by the simple acid texture exhibited regular periodic wrinkles whose periodicities were in a micro-scale. Two superhydrophobic surfaces with self-cleaning and high water adhesion were obtained. The resulting superhydrophobicity caused only by the topography changing instead of chemical modification. Owing to the silicon back bone in PDMS, the fabricated surface displayed mechanical stable superhydrophobicity under acidic and basic corrosive environments and a long duration.

The complicated rose petal topography manufactured by duplicating the close-packed polystyrene beads and acid corrosion process. The petal-like surface of superhydrophobicity and high adhesive force for water we fabricated had three structural levels including micro-convexes, nano-wrinkles and nanostructures. The resulting micro-convex, provided high-water adhesive ability due to van der Waals interaction, while nano-wrinkles and nanostructures provided superhydrophobicity caused by the lotus effect.

The unique property including superhydrophobicity and high-water adhesion was suitable for applying in liquid transportation. Unlike hairy type and tube type superhydrophobic surfaces, excessively strong adhesive force is disadvantageous to water-releasing. Furthermore, the fabricated material can use in future nonresidual imprint technique. We were firstly combined the “lotus effect” and “petal effect” to fabricate the nonresidual stamp. The stamp remained cleanly even though it was used for thousand times. From the point of applications, the technique we proposed is applicable in biotechnology, chemical engineering industry, and microfluidic devices.

Reference

Chapter 1

- [1] Z. Wang, G. Hang, Y. Wang, J. Li, W. Du, *Smart Mater. Struct.* **2008**, 17, 1.
- [2] M. Behl, A. Lendlein, *Soft Matter* **2007**, 3, 58.
- [3] J. O. Winter, T. Y. Liu, B. A. Korgel, C. E. Schmidt, *Adv. Mater.* **2001**, 13, 1673.
- [4] G. Ibarz, L. Dahne, E. Dönath, H. Mohwald, *Adv. Mater.* **2001**, 13, 1324.
- [5] I. Bontidean, A. Kumar, E. Csoregi, I. Y. Galaev, B. Mattiasson, *Angew. Chem. Int. Ed.* **2001**, 40, 2676.
- [6] H. Bayley, P. S. Cremer, *Nature* **2001**, 413, 226.
- [7] J. Liu, Y. Lu, *Adv. Mater.* **2006**, 18, 1667.
- [8] N. Willet, J. F. Gohy, L. Lei, M. Heinrich, L. Auvray, S. Varshney, R. Jerome, B. Leyh, *Angew. Chem. Int. Ed.* **2007**, 46, 7988.
- [9] F. Xia, L. Jiang, *Adv. Mater.* **2008**, 20, 2842.
- [10] L. Feng, S. Li, Y. Li, H. Li, L. Zhang, J. Zhai, Y. Song, B. Liu, L. Jiang, D. Zhu, *Adv. Mater.* **2002**, 14, 1857.
- [11] X. F. Gao, L. Jiang, *Nature* **2004**, 432, 36.
- [12] R. Blossey, *Nature Mater.* **2003**, 2, 301.
- [13] T. L. Sun, L. Feng, X. F. Gao, L. Jiang, *Acc. Chem. Res.* **2005**, 38, 644.
- [14] X. M. Li, D. Reinhoudt, M. Crego-Calama, *Chem. Soc. Rev.* **2007**, 36, 1350.
- [15] A. R. Parker, C. R. Lawrence, *Nature* **2001**, 414, 33.
- [16] Y. Zheng, H. Bai, Z. B. Huang, X. Tian, F. Nie, Y. Zhao, J. Zhai, L. Jiang, *Nature* **2010**, 463, 640.
- [17] K. Autumn, Y. A. Liang, S. T. Hsieh, W. Zesch, W. P. Chan, T. W. Kenny, R. Fearing, R. J. Full, *Nature* **2000**, 405, 681.
- [18] K. Autumn, M. Sitti, Y. A. Liang, A. M. Peattie, W. R. Hansen, S. Sponberg, T. W.

- Kenny, R. Fearing, J. N. Israelachvili, R. J. Full, *Proc. Natl. Acad. Sci. U.S.A.* **2002**, 99, 12252.
- [19] L. Qu, L. Dai, M. Stone, Z. Xia, Z. L. Wang, *Science* **2008**, 322, 238.
- [20] H. C. Von Baeyer, *Sciences-New York* **2000**, 40, 12.
- [21] R. Blossey, *Nat. Mater.* **2003**, 2, 301.
- [22] W. Barthlott, C. Neinhuis, *Planta* **1997**, 202, 1.
- [23] N. A. Patankar, *Langmuir* **2003**, 19, 1249.
- [24] Z. Yoshimitsu, A. Nakajima, T. Watanabe, K. Hashimoto, *Langmuir* **2002**, 18, 5818.
- [25] D. Quere, *Physica A* **2002**, 313, 32.
- [26] A. Lafuma, D. Quere, *Nat. Mater.* **2003**, 2, 457.
- [27] R. Furstner, W. Barthlott, C. Neinhuis, P. Walzel, *Langmuir* **2005**, 21, 956.
- [28] J. Shieh, F. J. Hou, Y. C. Chen, H. M. Chen, S. P. Yang, C. C. Cheng, H. L. Chen, *Adv. Mater.* **2009**, 21, 1.
- [29] I. P. Parkin, R. G. Palgrave, *J. Mater. Chem.* **2005**, 15, 1689.
- [30] J. De Coninck, M. J. de Ruijter, M. Voue, *Curr. Opin. Colloid Interface Sci.* **2001**, 6, 49.
- [31] T. Onda, S. Shibuichi, N. Satoh, K. Tsujii, *Langmuir* **1996**, 12, 2125.
- [32] M. Nosonovsky, B. Bhushan, *Adv. Funct. Mater.* **2008**, 18, 843.
- [33] P. G. de Gennes, F. Brochard-Wyart, D. Quere, *Capillarity and Wetting Phenomena-Drops, Bubbles, Pearls, Waves*; Springer: New York, 2002; p 216.
- [34] R. N. Wenzel, *Ind. Eng. Chem.* **1936**, 28, 988.
- [35] A. Cassie, S. Baxter, *Trans. Faraday Soc.* **1944**, 40, 546.
- [36] M. H. Sun, C. X. Luo, L. P. Xu, H. Ji, O. Y. Qi, D. P. Yu, Y. Chen, *Langmuir* **2005**, 21, 8978.
- [37] K. Koch, B. Bhushan, W. Barthlott, *Soft Matter* **2008**, 4, 1943.

- [38] B. Bhushan, Y. C. Jung, K. Koch, *Langmuir* **2009**, 25, 3240.
- [39] L. Feng, Y. Zhang, J. Xi, Y. Zhu, N. Wang, F. Xia, L. Jiang, *Langmuir* **2008**, 24, 4114.
- [40] J. Xi, L. Jiang, *Ind. Eng. Chem. Res.* **2008**, 47, 6354.

Chapter 2

- [1] L. Feng, S. Li, Y. Li, H. Li, L. Zhang, J. Zhai, Y. Song, B. Liu, L. Jiang, D. Zhu, *Adv. Mater.* **2002**, 14, 1857.
- [2] (a) T. Sun, L. Feng, X. Gao, L. Jiang, *Acc. Chem. Res.* 2005, 38, 644. (b) X. Feng, L. Jiang, *Adv. Mater.* **2006**, 18, 3063.
- [3] S. Wang, Y. Song, L. Jiang, *J. Photochem. Photobiol. C* **2007**, 8, 18.
- [4] M. Callies, D. Que' re', *Soft Matter* **2005**, 1, 55.
- [5] X. Zhang, F. Shi, J. Niu, Y. Jiang, Z. Wang, *J. Mater. Chem.* **2008**, 18, 621.
- [6] P. Roach, N. J. Shirtcliffe, M. I. Newton, *Soft Matter* **2008**, 4, 224.
- [7] L. Gao, T. J. McCarthy, *J. Am. Chem. Soc.* **2006**, 128, 9052.
- [8] Y. C. Jung, B. Bhushan, *Nanotechnology* **2006**, 17, 4970.
- [9] Z. Yoshimitsu, A. Nakajima, T. Watanabe, K. Hashimoto, *Langmuir* **2002**, 18, 5818.
- [10] X. Song, J. Zhai, Y. Wang, L. Jiang, *J. Phys. Chem. B* **2005**, 109, 4048.
- [11] M. Jin, X. Feng, L. Feng, T. Sun, J. Zhai, T. Li, L. Jiang, *Adv. Mater.* **2005**, 17, 1977.
- [12] Y. Zheng, X. Gao, L. Jiang, *Soft Matter* **2007**, 3, 178.
- [13] L. Gao, T. J. McCarthy, *Langmuir* **2006**, 22, 2966.
- [14] X. Gao, X. Yao, L. Jiang, *Langmuir* **2007**, 23, 4886.
- [15] Z. Cheng, L. Feng, L. Jiang, *Adv. Funct. Mater.* **2008**, 18, 3219.
- [16] X. Hong, X. Gao, L. Jiang, *J. Am. Chem. Soc.* **2007**, 129, 1478.

- [17] D. Huh, A. H. Tkaczyk, J. H. Bahng, Y. Chang, H. Wei, J. B. Grotberg, C. Kim, K. Kurabayashi, S. Takayama, *J. Am. Chem. Soc.* **2003**, 125, 14678.
- [18] W. Satoh, H. Hosono, H. Suzuki, *Anal. Chem.* **2005**, 77, 6857.
- [19] N. Yoshida, Y. Abe, H. Shigeta, A. Nakajima, H. Ohsaki, K. Hashimoto, T. Watanabe, *J. Am. Chem. Soc.* **2006**, 128, 743.
- [20] P. Dubois, G. Marchand, Y. Fouillet, J. Berthier, T. Douki, F. Hassine, S. Gmouh, M. Vaultier, *Anal. Chem.* **2006**, 78, 4909.
- [21] K. A. Wier, T. J. McCarthy, *Langmuir* **2006**, 22, 2433.
- [22] N. Zhao, Q. Xie, X. Kuang, S. Wang, Y. Li, X. Lu, S. Tan, J. Shen, X. Zhang, Y. Zhang, J. Xu, C. C. Han, *Adv. Funct. Mater.* **2007**, 17, 2739.
- [23] A. Lafuma, D. Que'ré', *Nat. Mater.* **2003**, 2, 457.
- [24] D. Que'ré', A. Lafuma, J. Bico, *Nanotechnology* **2003**, 14, 1109.
- [25] B. Bhushan, R. A. Sayer, *Microsyst. Technol.* **2007**, 13, 71.
- [26] B. Bhushan, A. G. Peressadko, T.-W. Kim, *J. Adhes. Sci. Technol.* **2006**, 20, 1475.
- [27] W. K. Cho, I. S. Choi, *Adv. Funct. Mater.* **2008**, 18, 1089.
- [28] D. Bargeman, *J. Colloid Interface Sci.* **1972**, 40, 344.
- [29] S. Boduroglu, M. Cetinkaya, W. J. Dressick, A. Singh, M. C. Demirel, *Langmuir* **2007**, 23, 11391.
- [30] M. H. Jin, X. J. Feng, L. Feng, T. L. Sun, J. Zhai, T. J. Li, L. Jiang, *Adv. Mater.*, **2005**, 17, 1977.
- [31] K. Autumn, Y. A. Liang, S. T. Hsieh, W. Zesch, W. P. Chan, T. W. Kenny, R. Fearing, R. J. Full, *Nature*, **2000**, 405, 681.
- [32] Y. Lai, X. F. Gao, H. Zhuang, J. Huang, C. Lin, L. Jiang, *Adv. Mater.* **2009**, 21, 3799.
- [33] J. B. West, *J. Appl. Physiol.* **1999**, 87, 1543.

- [34] X. Huang, D. Kim, M. Im, J. Lee, J. Yoon, Y. Choi, *small* **2009**, 5, 90.
- [35] J. Xi, L. Jiang, *Ind. Eng. Chem. Res.* **2008**, 47, 6354.
- [36] E. Bormashenko, T. Stein, R. Pogreb, D. Aurbach, *J. Phys. Chem. C* **2009**, 113, 5568.
- [37] M. Liu, Y. Zheng, J. Zhai, L. Jiang, *Accounts Chem. Res.* **2010**, 43, 368.
- [38] Y. M. Zheng, X. Gao, L. Jiang, *Soft Matter* **2007**, 3, 178.

Chapter 4

- [1] N. Bowden, S. Brittain, A. G. Evans, J. W. Hutchinson, G. M. Whitesides, *Nature* **1998**, 393, 146.
- [2] T. Okayasu, H. L. Zhang, D. G. Bucknall, G. A. D. Briggs, *Adv. Funct. Mater.* **2004**, 14, 11, 1081.
- [3] P. Jothimuthu¹, A. Carroll¹, A. A. S Bhagat¹, G. Lin, J. E Mark, I. Papautskyl, *J. Micromech. Microeng.* **2009**, 19, 045024.
- [4] R. N. Wenzel, *Ind. Eng. Chem.* **1936**, 28, 988.
- [5] A. Cassie, S. Baxter, *Trans. Faraday Soc.* **1944**, 40, 546.
- [6] H. M. Whitney, L. Chittka, T. J. A. Bruce, B. J. Glover, *Current Biology* **2009**, 19, 1.
- [7] N. D. Denkov, O. D. Velev, P. A. Kralchevsky, I. B. Ivanov, H. Yoshimura, K. Nagayama, *Nature* **1993**, 361, 26.
- [8] P. G. de Gennes, F. Brochard-Wyart, D. Quere, *Capillarity and Wetting Phenomena-Drops, Bubbles, Pearls, Waves*; Springer: New York, 2002; p 218.
- [9] L. Feng, Y. Zhang, J. Xi, Y. Zhu, N. Wang, F. Xia, L. Jiang, *Langmuir* **2008**, 24, 4114.